



## Deliverable Report for Grant Agreement Number 760813

### Deliverable 4.5

## COMPARE AND CONTRAST 3D GIT AND LIVER TO CROSS-SPECIES MODELS

**Due date of deliverable: 28/02/2021**

**Actual submission date: 25/02/2021**

**Lead beneficiary for this deliverable: SU**

**Contributing beneficiaries for this deliverable: HWU, IUF, UNEXE, UL**

Dissemination Level:		
PU	Public	X
PP	Restricted to other programme participants (including the Commission Services)	
RE	Restricted to a group specified by the consortium (including the Commission Services)	
CO	Confidential, only for members of the consortium (including the Commission Services)	

## TABLE OF CONTENTS

<b>1. Description of task</b>	<b>3</b>
<b>2. Description of work &amp; main achievements</b>	<b>3</b>
<b>2.1 Comparing and contrasting 3D liver models to cross-species models</b>	<b>3</b>
2.1.1 Mapping the molecular underpinnings for AOPs for oxidative responses to metal based ENMs in zebrafish against mammals	<b>6</b>
2.1.2 Conclusions	<b>10</b>
<b>2.2 Comparing and contrasting advanced GIT models to cross-species models</b>	<b>11</b>
2.2.1 <i>In vitro</i> and <i>in vivo</i> microbiome related studies and comparisons	<b>11</b>
2.2.2 Zebrafish cross-species comparison studies - Zebrafish larva microbiota	<b>17</b>
2.2.3 Zebrafish cross-species comparison studies - Adult Zebrafish oral exposure studies	<b>22</b>
2.2.4 Conclusions	<b>24</b>
<b>2.3 References</b>	<b>25</b>
<b>3. Deviations from the Workplan</b>	<b>27</b>
<b>4. Performance of the partners</b>	<b>27</b>
<b>5. Conclusions</b>	<b>28</b>
<b>6. Annex</b>	<b>28</b>
<b>Annex 1:</b> Molecular Initiating Events (MIEs) / Key Events (KEs), biomarkers and assays for PATROLS-relevant liver AOPs	<b>29</b>
<b>Annex 2:</b> Additional data to support Section 2.1.1 Mapping the molecular underpinnings for AOPs for oxidative responses to metal based ENMs in zebrafish against mammals	<b>43</b>
<b>Annex 3:</b> Supporting <i>in vitro</i> GIT model data following ENM exposure in the presence or absence of the microbial metabolite butyric acid	<b>51</b>

## 1. Description of task

### **Task 4.5 Compare and contrast 3D GIT and liver models to cross-species models; (SU, IUF, HWU); M25-37.**

Task 4.5 will contribute to the interspecies toxicity extrapolation models of Task 5.3. Task 4.5 will choose one gut model (HWU) and one liver model (SU) for comparison with the gut and liver responses of the zebrafish to specific ENM. The data generated from Tasks 4.1-4.4 will be transferred to WP5 to facilitate this cross-species comparison. A GIT model incorporating microflora components or metabolites will be prioritised for comparison with the effects of dietary ENM on zebrafish gut microbiota and concurrent neutrophil and macrophage responses. Task 4.5 will coordinate with Task 5.3 to use similar standard bioassays for (pro-)inflammatory (e.g. cytokine/chemokine expression) and oxidative stress (e.g. glutathione depletion). A primary objective will be to identify overlaps in responses across models to enhance ability for extrapolation. In addition to the standard bioassays, bioassays based on overlaps between the AOPs of rodent and zebrafish models will be used to identify and prioritise common novel bioassays suitable for both fish and humans. These priority bioassays will be developed in conjunction with WP3 and WP5.

## 2. Description of work & main achievements

### **2.1 Comparing and contrasting 3D liver models to cross-species models (SU, UNEXE)**

At the start of this task in Jan 2020, SU coordinated a joint half-day workshop with participants from WP3, 4 and 5 to discuss the linkage between the respective tasks dedicated to exploring the possibility of cross-species models to predict mammalian hazard responses. UNEXE (Task 5.2 and 5.3 lead) prepared an overview of the experimental work conducted in zebrafish, which focused on findings from the use of a transgenic fluorescence reporter system for detecting oxidative stress which is a key mechanism by which ENM induce cellular damage. The zebrafish model detects oxidative responses through the electrophile response element- EpRE (Mourabit et al, 2019), and applied with embryo-larvae it is possible to detect whole organism responses using imaging methods. Use of this transgenic zebrafish model as part of WP5 following exposure to ENM identified dose-dependent and tissue specific effects. The transgenic reporter system thus provided an opportunity to explore correlations with responses observed in mammalian cell systems, particularly the *in vitro* liver models applied in WP4. Immunological responses (macrophage and neutrophil responses) were also studied within WP5 using a series of other transgenic zebrafish models (UNEXE and UL), but the nature of those studies differed in terms of the purpose of the work compared with those conducted in WP4, making direct comparisons difficult. Specifically, studies in WP4 focused on long-term

exposures to ENMs in the *in vitro* models to assess immunological responses whereas studies using the transgenic zebrafish were focused on short term exposures as part of a work programme focused on generating knowledge on which tissues/organs were the most sensitive to the exposed materials. The work on zebrafish in WP5 lead to investigations into the chronic effects of ENMs on sensory systems including olfaction, responses in neuromasts (sensory cells, which detect water movement by deflection of cilia, and associated support and mantle cells) and ion regulatory systems, rather than immunological function.

Through these initial discussions, it was decided that it would be important to address the following questions to establish the applicability domain for cross-species models in predicting human health outcomes:

- How do the main target tissues in the different species compare and are there common functional consequences (AOPs);
- In what ways are the genes and pathways for oxidative stress conserved across species;
- Can responses for oxidative stress seen in zebrafish (or other species) be usefully applied (as surrogates) to predict for effects in mammals/humans?

To address these questions in relation to the liver, it was vital to transfer data generated from Tasks 4.1-4.4 (SU, HWU, IUF, InSphero, Misvik, UL) to WP5 in order to facilitate cross-species comparisons. To make decisions on which data should be transferred from WP4 to WP5 with respect to the liver models, summary tables listing all *in vitro* models (including information on cell types) and endpoints evaluated, linked to current understanding of human AOPs were shared with WP5 (**Annex 1**). These summary tables were the basis of the activity under Task 2.5 as reported in PATROLS **Deliverable 2.5**.

The summary tables were reviewed by UNEXE to identify cell types of importance to allow for linkage between the WP4 and WP5 data sets, possible endpoint overlaps between the zebrafish and *in vitro* liver model ENM testing approaches that could facilitate cross-species comparisons and data gaps that may need to be addressed. The outcome of this analysis is summarised in **Table 1**.

**Table 1: Summary of cross-species linkage analysis focusing on oxidative responses seen in zebrafish being applied (as surrogates) to predict for effects in humans.**

Mammals	Targets	Similar cells in fish
Liver inflammation Liver fibrosis	<b>Liver cells,</b> Oxidative stress – via gene systems Inflammation- ILs , NfκB etc. Mitochondrial dysfunction Cell injury/death As above +	<b>Liver cells</b> All measurable and parallels occur in fish <b>(adults)</b> Liver <b>ROS induction (EpRE)</b> How do we distinguish fibrosis vs inflammatory responses – <b>stage?</b>
Liver cancer	<b>Liver cells</b> ROS, DNA damage, DNA adducts, whole series of gene targets p53, p72 etc	<b>Liver cells</b> All measurable and parallels occur in fish <b>(adults)</b> Embryo-larvae- <b>Liver ROS induction (EpRE)</b>

From this first stage of the analysis, it was clear that whilst hepatic response to ENMs is data rich for human cells in PATROLS, there are far less data for wildlife species. Furthermore, for the studies in zebrafish (the most commonly adopted fish model for laboratory-based studies on ENMs), there have been few reported studies focused on investigating responses specifically within the liver. Most of the studies conducted to date on ENMs in zebrafish have been carried out on embryos and/or early larval stages and thus effects have tended to be systemic evaluations as opposed to those on specific tissues. Molecular responses (including the few transcriptomic analyses) too have focused on whole body responses rather than on dissected liver tissue largely because of the very small size of the zebrafish embryo-larvae. This complicates a direct comparison between the data generated in WP4 on ENM exposure to advanced *in vitro* human cell culture models and equivalent data sets in fish. Whilst there was overlap in the endpoints considered in both WP4 and WP5 (e.g. (pro-)inflammatory (e.g., cytokine/chemokine expression) and oxidative stress (e.g., glutathione depletion)), the lack of liver tissue specificity in the zebrafish embryo analysis in WP5 prevented direct comparison with the cellular and molecular responses generated from the laboratory studies in WP4 on mammalian cells.

One clear common finding between the studies conducted for the *in vitro* liver models from WP4 and the ecological species evaluations undertaken in WP5 for ENM, however, was for activation of pro-inflammatory and oxidative stress response pathways and their association

with AOPs across the species. Thus, using informatics approaches, we set out to determine if the genes and pathways for oxidative stress induced by an array of different ENM were conserved across species.

### 2.1.1 Mapping the molecular underpinnings for AOPs for oxidative responses to metal based ENMs in zebrafish against mammals (UNEXE)

This work set out to establish the conservancy in responses of selected gene pathways and molecular targets for metal based ENMs in zebrafish to their equivalents in the human genome.

A preliminary survey of all the available literature identified a number of possible adverse effects of metal based ENMs on fish, including oxidative stress, inflammation, respiratory distress, inhibition of Na<sup>+</sup>K<sup>+</sup>-ATPase, neurological damage and defects in embryo development. Oxidative stress, however, is widely recognised as a predominant effect (Mendoza & Brown, 2019). Analysis for ENM gene activation focused on ZnO and Ag, as most data were available for these materials and they are recognised as amongst the most reactive metal based ENMs. This analysis identified a key set of genes in zebrafish that are established to be conserved across vertebrate species (**Table** ).

**Table 2: Selected conserved genes regulated in response to oxidative stress in zebrafish derived from literature.**

Genes	ID
<b>catalase</b>	CAT
<b>glutathione peroxidase</b>	GPx
<b>glutathione S-transferase</b>	GST
<b>superoxide dismutase</b>	SOX
<b>glutathione</b>	GSH
<b>superoxide dismutase</b>	SOD
<b>glutathione reductase</b>	GR
<b>mitogen activ. prot. kinase</b>	MAPK
<b>peroxiredoxin</b>	Prx
<b>thioredoxin peroxidase</b>	Trx
<b>heat-shock factor</b>	HSF

<b>nuclear factor erythroid 2–related factor 2</b>	Nrf2, nfe2l2a
<b>nuc. factor κ-light-chain-enhancer of act. B cells</b>	NF-κB
<b>metal transcription factor</b>	MTF
<b>hypoxia inducible factor</b>	HIF
<b>aryl–hydrocarbon receptor</b>	AhR
<b>tumor protein p53</b>	P53

Relating to the genes identified in **Table 2**, in mammals and fish, three intramitochondrial, H<sub>2</sub>O<sub>2</sub> consuming pathways are recognised as commonly shared: catalase, glutathione-dependent peroxidases and thioredoxin dependent peroxidases (also known as peroxiredoxins; Banh *et al.*, 2016). Activation of these genes and their associated functional pathways differs depending on the dosing level of the ENM (and induced severity of the oxidative stress). For example, mild oxidative stress induces transcriptional activation of phase II antioxidant enzymes via Nrf2 induction, intermediate levels induce a proinflammatory response through redox-sensitive MAPK and NF-κB cascades, whereas highly toxic levels result in mitochondrial membrane damage and electron chain dysfunction leading to cell death (Manke *et al.*, 2013). Studies specifically on the effects of AgNPs in liver tissues of zebrafish have been shown to influence the pathway related to glutathione regulation. It is important to recognise also that some of these genes identified can result in the activation of different functional pathways and response mechanisms, complicating thorough understanding of the shared response systems and mechanism between species. As an example, exposure to ZnO induced ROS can trigger the p53 gene which triggers expression of various antioxidant genes including SOD2, GPX1, SESN1, SESN2 and ALDH4A1 to restore oxidative homeostasis (Setyawati *et al.*, 2013). Nevertheless, this analysis of the available literature clearly identifies common target genes between fish and mammals that are conserved in their responses to metal based ENMs that map to oxidative response pathways and with utility not only as biomarkers of exposure across species but also for assessing commonality in effect mechanisms, including specifically in the liver.

In the next phase of this work, we sought to take a less biased approach for assessing response mechanisms to ENM between mammals and zebrafish through the application of genome wide approaches. Here we set out to identify orthologues and their ontologies, map these genes to organs (here, the liver) and then map those genes to pathways associated with oxidative stress.

### Mapping of zebrafish orthologues

While orthologues are more likely to have the same functions across species, it is also possible that their functions are fulfilled by different genes. We therefore first sought to apply genome wide analyses to investigate this for the zebrafish in an attempt to more fully map the oxidative molecular responses across species. To do so, the functional annotations from the zebrafish orthologues (GCA\_000002035.4) were established using the UniProtKB and UniParc databases (“UniProt: a worldwide hub of protein knowledge,” 2019). This analysis was conducted as part of an analysis in WP5 (**Deliverable 5.2**) that included also *Daphnia magna* (GCA\_003990815.1) and *Raphidocelis subcapitata* (an algae, GCA\_003203535.1) for the wider cross species analysis of the conservation of these targets. We used custom Python scripts to establish similarity of the annotated genes. Additional support for the functional assignment for orthologues of interest identified in zebrafish, was derived from searches on other fish species with whole genome sequences available (and where most of their genes are annotated). These species included *Gasterosteus aculeatus* (three-spined stickleback, GCA\_006229165.1), *Oryzias latipes* (Japanese medaka, GCA\_002234675.1), *Tetraodon nigroviridis* (spotted green pufferfish, GCA\_000180735.1) and *Takifugu rubripes* (torafugu, GCA\_901000725.2) (Cossins & Crawford, 2005).

### Mapping of genes/orthologues to oxidative responses in liver

The UniProtKB/UniParc databases were then used to find all the genes expressed in the liver of all the species considered, and this found 35,094 genes. This list was then filtered using custom Python scripts for matches with the previously identified full list of zebrafish orthologues to identify 15,423 unique annotations for liver. This list was used to isolate 2,964 genes shared across zebrafish and mammals, using functional annotations and gene names. Interrogating this last list with annotations and gene names involved in oxidative stress response, identified 101 genes in the mammalian liver involved in oxidative stress response (**Annex 2, Supplementary Table S1**).

### Mapping of gene pathways

The last objective of this piece of informatics work was to map the identified 101 liver genes to their associated regulatory networks or pathways. The KEGG database (Kanehisa, 2000) provides known pathways and functional annotations for mammals against which other species can be compared. Using custom Python scripts, the gene lists for zebrafish were grouped by pathway, then sorted by functional annotation. For oxidative stress, 4 pathways (**Table 3**)

showed strong commonality for: “oxidative phosphorylation” (KEGG ID 190), “glutathione metabolism” (KEGG ID 480) (represented in **Figure 1**), “MAPK signalling” (KEGG ID 4010), and “P53 signalling” (KEGG ID 4115) (**Annex 2, Supplementary Figure S1–S4**).

**Table 3: Number of shared genes from all the species considered in functional pathways relating to oxidative stress between mammals and zebrafish.**

Pathway	No. of shared genes
<b>oxidative phosphorylation</b>	146
<b>glutathione metabolism</b>	67
<b>MAPK signaling</b>	408
<b>P53 signaling</b>	88

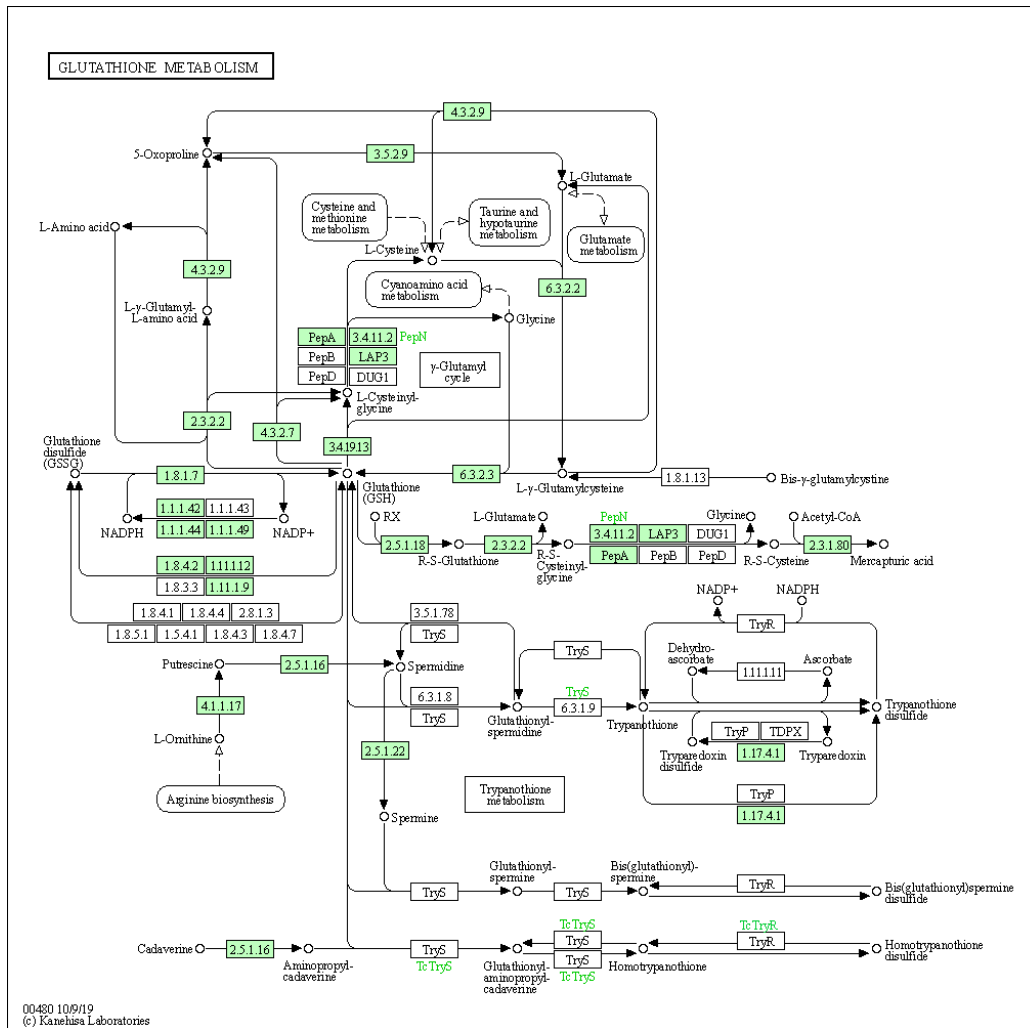


**Figure 1: KEGG pathway of glutathione metabolism (KEGG ID 480); the genes in green are present in *Danio rerio*.**

### 2.1.2 Conclusions

Adopting informatics approaches through interrogation of genome sequence information, we show strong cross species similarities between mammals and zebrafish in the gene pathways and regulatory networks associated with oxidative responses, a major effect pathway for metal based ENMs. For the liver, these response pathways included oxidative phosphorylation, glutathione metabolism, MAPK signalling and P53 signalling. These findings strongly support the use of zebrafish for predicting adverse outcomes in mammals associated with exposure to ENMs and for understanding the major common regulatory and functional networks associated with oxidative stress mechanism for ENM exposures.

## 2.2 Comparing and contrasting advanced GIT models to cross-species models (IUF, UL, HWU)

### 2.2.1 *In vitro* and *in vivo* microbiome related studies and comparisons (IUF)

In WP4, the IUF has developed an intestinal triple culture model – combining Caco-2, HT29-MTX-E12 and THP-1 cells – which can be applied in a state resembling the healthy organ (“Stable triple culture model”, **Deliverable 4.1**) or the inflamed intestine (“Inflamed triple culture model”, **Deliverable 4.2**). Using the PATROLS Tier 1 engineered nanomaterials (ENM), *i.e.*, specifically polyvinylpyrrolidone-capped silver (Ag-PVP) and titanium dioxide (TiO<sub>2</sub>), the toxic effects were compared between the *in vitro* models and *in vivo* feeding studies using the same materials (WP2). Overall, effects in the investigated endpoints were minimal. No adverse effects were detected in the intestinal tissue of exposed mice regarding DNA damage, oxidative stress or DNA repair (detailed in **Deliverable 2.3**). Similarly, ENM exposure did not cause cytotoxicity, DNA damage or pro-inflammatory responses *in vitro* (full experimental description and results are reported in **Deliverables 4.1** and **4.2**).

As the PATROLS-organised AOP workshop (Task 2.5) resulted in the outcome that no gut-specific AOPs are available, efforts were focused on the identification of new/additional markers to facilitate *in vivo-in vitro* extrapolation attempts. In this context, the expression of mucins, especially mucin (MUC/muc)2 emerged as a promising lead (as detailed in **Deliverable 4.3**). In both the intestinal tissue of Ag-PVP-fed mice and chronically exposed inflamed triple cultures, the expression of MUC/muc2 was significantly reduced. In acutely treated stable triple cultures, the same tendency was detected, but the results failed to reach statistical significance. Additional work was conducted to identify further markers for *in vivo-in vitro* comparisons on protein level. To achieve this, small intestinal tissue samples from control mice and animals suffering from dextran sulphate sodium (DSS)-induced colitis were analysed using a cytokine protein array and compared to the results from stable and inflamed *in vitro* triple cultures (RnD Systems, Proteome Profiler cytokine array kit for mouse or human). For the *in vitro* models, additional analyses were performed on samples following acute exposure to Ag-PVP or TiO<sub>2</sub> ENM.

To further investigate the potential effects of the mucin changes *in vivo*, the microbiome was analysed. As before, the detected changes were minimal (**Deliverable 2.3**). Nevertheless, the microbiome analysis offered an additional opportunity to (1) enable cross-species extrapolation with zebrafish (WP5), and to (2) consider *in vivo-in vitro* extrapolation. To account for the potential impact of the microbiota on ENM-induced effects, the intestinal *in vitro* models were

established and exposed in the presence of butyric acid. Butyric acid is one of the most prominent microbial metabolites in the gut and well known for its beneficial role in intestinal health (Borycka-Kiciak *et al*, 2017; Załęski *et al*, 2013). In the context of the 3Rs principles and the aim to ultimately replace animal research with *in vitro* models, this complex relationship between intestinal health and integrity, microbial populations, and xenobiotics needs to be addressed in view of ENM-microbiome interactions.

### 2.2.1.1 Results

***In vivo***: The effects of oral exposure to different ENM (*i.e.*, cerium oxide [CeO<sub>2</sub>], amorphous silica [SiO<sub>2</sub>], Ag-PVP and TiO<sub>2</sub>) on the murine microbiome was analysed using next generation sequencing (NGS). The samples were generated in feeding studies using female C57BL/6J mice that had been exposed to CeO<sub>2</sub> (NM-212) and amorphous SiO<sub>2</sub> (SAS) (21 days feeding studies), as well as female and male C57BL/6J mice exposed to Ag-PVP (Sigma) and TiO<sub>2</sub> (p25) in feed pellets (28 days feeding). For the analysis, DNA was isolated from faecal samples. The  $\alpha$ -diversity was determined as a measure of the intrinsic diversity of each individual sample. Besides the richness, the evenness was investigated in the form of Shannon entropy and Simpson's index. Furthermore, the  $\beta$ -diversity was computed according to weighted UniFrac analysis. Differences of abundance between control and exposure groups were then studied on the taxonomic levels of phylum and genus.

Overall, the ENM-induced effects in the microbiome were small. For none of the investigated ENM a change in  $\alpha$ -diversity was detected. Interestingly, however, a difference in  $\beta$ -diversity was measured between male and female mice treated with Ag-PVP and TiO<sub>2</sub> ENM, which suggests that a consideration of both sexes might be crucial for further microbiome studies. This observation may be of particular importance in the discussions on the replacement of *in vivo* studies with *in vitro* approaches. In this regard, the review of organisms typically applied in ecotoxicity testing, *e.g.*, zebrafish, might offer a more suitable alternative.

Specific effects of the ENM on the mouse microbiome on phylum or genus level were rare. The exposure to SiO<sub>2</sub> was associated with a reduced relative abundance of *Actinobacteria* – a phylum of crucial importance for gut homeostasis (Binda *et al*, 2018). A particular genus belonging to this phylum – *i.e.*, *bifidobacterium* – is prominently associated with intestinal health and alterations frequently reported in intestinal pathologies (Tojo *et al*, 2014). For Ag-exposed female mice, an increase in the relative abundance of *Roseburia* was detected, a genus

which has been linked to ant-inflammatory responses in the intestine.<sup>1</sup>

***In vitro***: For most biological laboratories, the culture of live bacterial cultures is a logistic challenge. Furthermore, establishing co-cultures while preventing bacterial overgrowth is difficult to achieve without the incorporation of additional parameters, *e.g.*, flow. Therefore, the presence of microbiota was mimicked by incorporation of butyric acid, a well-known microbial metabolite.

The effects of ENM were investigated in presence of 1 mM butyric acid (BA) using two *in vitro* systems: proliferating monocultures of Caco-2 and HT29-MTX-E12 (hereinafter “E12”) cells as well as triple cultures of Caco-2, E12, and THP-1 cells in healthy and inflamed state (SOPs in **Deliverables 4.1** and **4.2**). In monoculture experiments, ENM exposure was tested using either pristine or artificially digested particles suspended in foetal bovine serum (FBS)-reduced culture medium.

### *Monocultures*

In proliferating monocultures (**Figure 2 & Annex 3, Figure S1**), the effect of BA co-incubation varied considerably between the investigated cell lines and tested ENM. For Ag-PVP ENM (**Annex 3, Figure S1**), the simulation of digestion did not alter the toxicity. Regardless of the condition, no cytotoxicity was noted in E12 cells for exposure concentrations up to 80  $\mu\text{g cm}^{-2}$  Ag-PVP. In Caco-2 cells, the Ag-PVP-induced toxicity was delayed to a higher concentration in presence compared to absence of BA.

Amine-modified polystyrene (PS-NH<sub>2</sub>) ENM exerted strong cytotoxicity in both Caco-2 and E12 cells (**Figure 2**), starting from 1 and 10  $\mu\text{g cm}^{-2}$ , respectively. The presence of BA resulted in cell line-specific effects. In Caco-2 cells, the PS-NH<sub>2</sub>-induced toxicity was significantly reduced for lower exposure concentrations in presence of BA (**Figure 2, A, B**).

E12 cells were overall more robust towards PS-NH<sub>2</sub> ENM exposure (**Figure 2, C, D**). The presence of BA did not impact the particle-induced cytotoxicity consistently.

---

<sup>1</sup> 10.1111/jgh.14144

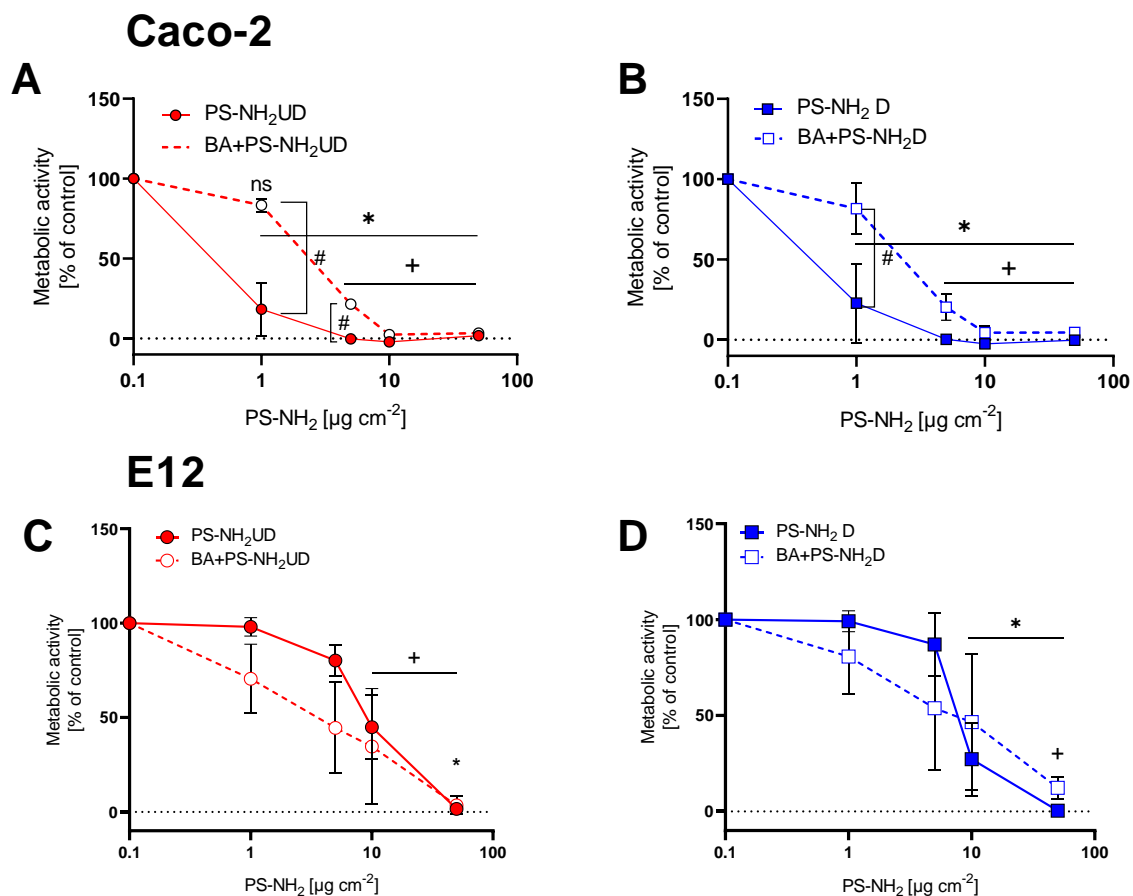


**Figure 2. Metabolic activity after 24h exposure to undigested and digested PS-NH<sub>2</sub> ENM with and without co-incubation with 1 mM BA.** (A) Caco-2 cells exposed to undigested PS-NH<sub>2</sub>, (B) Caco-2 cells exposed to digested PS-NH<sub>2</sub>, (C) E12 cells exposed to undigested PS-NH<sub>2</sub> (D) E12 cells exposed to digested PS-NH<sub>2</sub> (average  $\pm$  SD of N=3, \* $p \leq 0.05$  without BA incubation compared to corresponding control; + $p \leq 0.05$  cultures with BA incubation compared to corresponding control; # $p \leq 0.05$  compared to corresponding exposure concentration without BA incubation. Statistical analysis with One-way ANOVA and Bonferroni *post hoc* test.)

### Triple cultures

Before ENM exposure experiments were conducted, the general effect of BA on the stable and inflamed triple culture model was investigated. The results on barrier integrity, DNA damage and cytokine release were detailed in **Deliverable 4.2**. The outcomes regarding LDH release are shown in **Figure 3** below. Establishing the triple cultures in the presence of 1 mM BA marginally affected the barrier integrity over 48h of culture. However, no significant differences between BA co-incubated and control cultures were detected for any of the investigated endpoints.

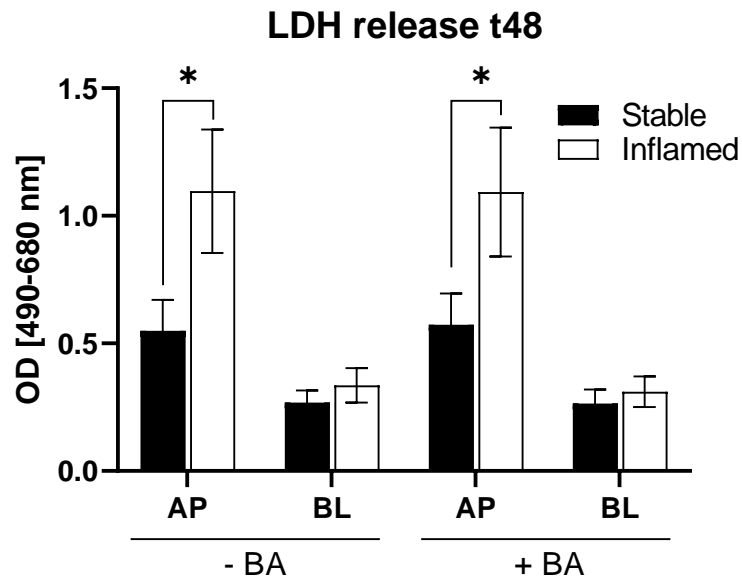


**Figure 3. LDH release after 48h stable and inflamed triple culture** in absence and presence of 1 mM BA (Average  $\pm$  SD of N=3, \* $p \leq 0.05$  compared to the corresponding stable condition. Statistical analysis by One-way ANOVA and Tukey's *post hoc* test.)

Subsequently, the stable and inflamed models were set-up with 1 mM BA and exposed to PS-NH<sub>2</sub> ENM for 24h. Whereas no effect on the barrier integrity (**Annex 3, Figure S2**) or cytokine release (interleukin 1 $\beta$ , 8, 6 and tumour necrosis factor alpha; **Deliverable 4.2**) was noted, the LDH release caused by the PS-NH<sub>2</sub> exposure was substantially reduced in BA-incubated stable triple cultures and failed to reach statistical significance (**Annex 3, Figure S3**).

#### *Protein array analysis – in vivo vs in vitro*

Of stable and inflamed triple cultures, all cell types, *i.e.*, the epithelial cells on the transwell filter and the THP-1 macrophage-like cells, were pooled for the analysis. In total, 105 different proteins were analysed and compared using the proteome profiler. Around two third of these proteins were enhanced in the inflamed compared to the stable triple culture (**Annex 3, Figure S4**). However, five cytokines that were upregulated in the inflamed model stood out more prominently – chemokine ligand 13 (CXCL13), growth-arrest-specific (GAS)-6, and the interleukins (IL)-2, IL-5, and IL-23.

All five cytokines have been demonstrated to be implicated in intestinal inflammation (Rothlin *et al*, 2014; Fuss *et al*, 1996; Singh *et al*, 2016).

The *in vitro* outcomes were compared to intestinal tissue of healthy control mice as well as mice that were subjected to the induction of colitis using DSS. Clear differences in the protein profiles were evident using of the murine-equivalent cytokine array kit. In total, 16 proteins were significantly changed following DSS-induced colitis (**Figure 4**).

An overlap between the *in vivo* and *in vitro* results was determined for 11 out of these 16 proteins, including macrophage inflammatory protein (MIP)-3 $\alpha$ , IL-23, and TNF- $\alpha$ .

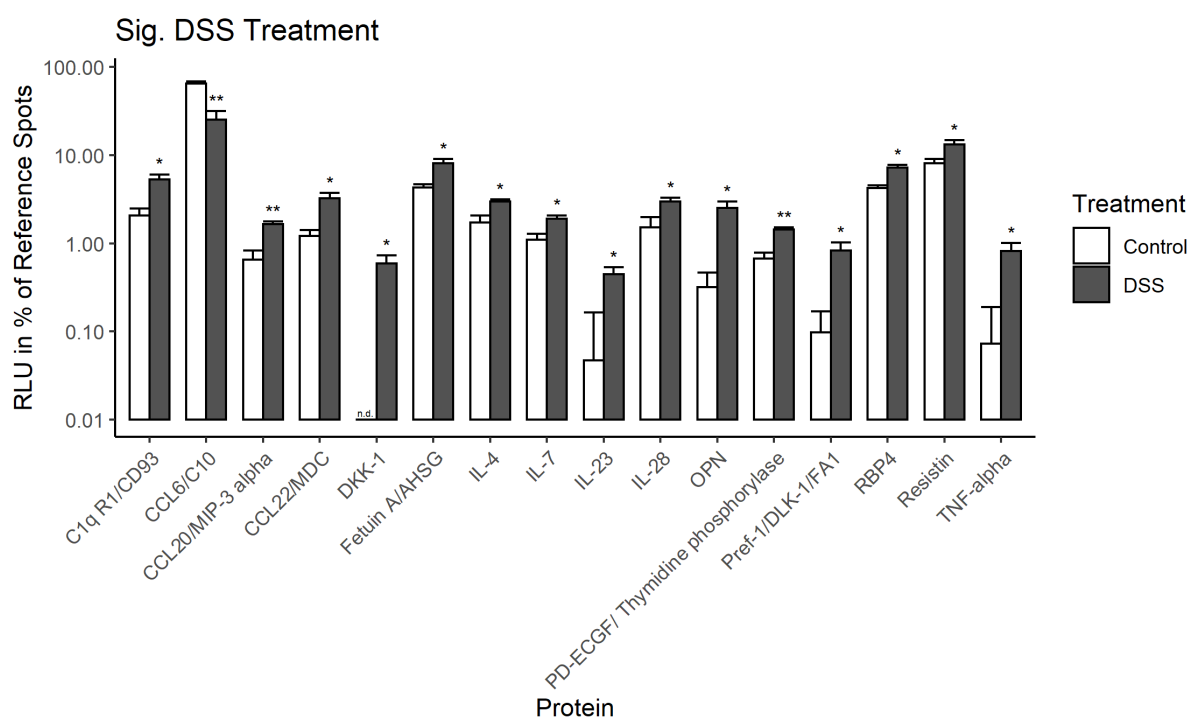


**Figure 4. Significantly changed proteins in intestinal tissue of mice after DSS-induced colitis** (n=3; Average  $\pm$  SEM; \* $p \leq 0.05$ , \*\* $p \leq 0.01$  compared to the control. Statistical analysis with t-test).

#### *Protein array analysis – stable and inflamed triple cultures after exposure to ENM*

Stable and inflamed triple cultures were acutely exposed to Ag-PVP or TiO<sub>2</sub> ENM (80  $\mu\text{g}/\text{cm}^2$ ) for 24h. Preliminary results suggest that both in the stable and inflamed model the effects of Ag-PVP and TiO<sub>2</sub> ENM differed.

These initial semi-quantitative results do not yet allow conclusions on specific ENM-induced effects but offer a basis for further investigation and validation using more specific, quantitative analyses of individual cytokines. In addition, murine intestinal tissue of animals that were

exposed to these nanomaterials in feed pellets are available, which offers the opportunity for *in vivo-in vitro* comparison.

### 2.2.2 Zebrafish cross-species comparison studies - Zebrafish larva microbiota studies (UL)

At Leiden University (UL), the acute effects of the ENMs TiO<sub>2</sub> (NM-105) and Ag (NM300-K) on microbiota were studied in zebrafish embryos and larvae.

Early zebrafish development includes different stages. Most tissues and organs are formed during the embryonic life stage, which ends at the time of hatching, a classical endpoint in acute toxicity tests. Laboratory strains of zebrafish hatch around 2-3 days post fertilization (dpf). After the embryonic period, larvae still obtain energy from their yolk; it takes some days (until ~3 dpf at 28.5°C) before they open their mouth (defined as the protruding mouth stage). Subsequently, the immune system matures until 2-4 weeks post-fertilization, and zebrafish reach sexual maturity around 3 months post-fertilization.

Within our study, the embryonic (egg) stage and larval stages up to 6 dpf have been studied. At these early life stages, zebrafish acquire microbiota from the water on their chorion (pre-hatching) and epidermis (post-hatching). The opening of the larvae's mouth marks the onset of microbial colonization of the intestinal lumen. Given the initial colonization of external surfaces of zebrafish embryos and larvae, aqueous exposure conditions were selected for all experiments (summarized in **Table 4**.) The effects of Ag NPs on adult zebrafish microbiota have previously been studied under aqueous exposure, as reported by Ma et al. (2018). The results of this study will be reported for comparison with the microbiota studies with mice performed by IUF (described above in Section 2.2.1).

**Table 4. Summary of the aqueous exposure conditions in embryonic, larval and adult zebrafish studies.**

Exposure characteristics	Zebrafish embryos (WP5)	Zebrafish larvae (WP5)	Zebrafish adults (Literature; Ma et al., 2018)
<b>Particles</b>	TiO <sub>2</sub> NPs (NM-105)	AgNPs (NM 300-K)	AgNPs from Sigma-Aldrich (CAS 7440-22-4)
<b>Concentrations</b>	0, 2, 5, 10 mg TiO <sub>2</sub> ·L <sup>-1</sup> (nominal)	0, 0.25, 0.75, 1, 1.5, 2.5 mg Ag·L <sup>-1</sup> (nominal); 0, 0.20±0.02, 0.74±0.008, 0.89±0.02, 1.49±0.02, 1.53±0.06 mg Ag·L <sup>-1</sup> (actual/particulate)	0, 10, 33, 100 µg Ag·L <sup>-1</sup> (nominal) 4.5±0.3 and 5.3±0.3, 18.3±1.2 to 19.5±1.2, and 45.1±2.0 to 49.2±4.3 µg·L <sup>-1</sup> (actual/total)
<b>Duration</b>	24h	48h	35d
<b>Medium replacement</b>	None	Daily	Daily: half of the exposure water; weekly: all exposure water.
<b>Exposed life stage</b>	0-1 dpf larvae	3-5 dpf larvae	3 months old adults
<b>Final particle burden</b>	30.4±9.0 ng·egg <sup>-1</sup> (at 2 mg·L <sup>-1</sup> exposure) 154.3±19.2 ng Ti·egg <sup>-1</sup> (at 5 and 10 mg TiO <sub>2</sub> ·L <sup>-1</sup> )	Not determined	0, 14.4±0.5, 37.8±2.2, 69.0±4.6 µg Ag·g <sup>-1</sup> intestine (males) 0, 15.7±1.5, 36.2±1.5, 68.1±3.9 µg Ag·g <sup>-1</sup> intestine (females)

### 2.2.2.1 Zebrafish embryos microbiota studies

The experiments performed with zebrafish embryos focused on the hypothesis that the adsorption of nanoparticles (NPs) on the eggs' external chorion membrane interferes with the initial microbial colonization of the chorion, and with the subsequent colonization of the post-hatch larvae. To test this, zebrafish eggs were exposed from 0-1 dpf to 0, 2, 5 and 10 mg TiO<sub>2</sub>·L<sup>-1</sup>. Particle adsorption on the chorion saturated at the 5 mg TiO<sub>2</sub>·L<sup>-1</sup> exposure, as determined using particle-induced X-ray analysis. For this reason, the effects TiO<sub>2</sub> NPs on microbiota were characterized at this exposure concentration. Confocal microscopy imaging with dead/total fluorescent cell staining (propidium iodide/Syto-9), revealed that TiO<sub>2</sub> exposure resulted in higher dead and total microbial abundance on the chorion (dead coverage: 0.28 ± 0.05% vs. 0.14 ± 0.01%; and total coverage: 0.50 ± 0.10% vs. 0.43 ± 0.06%). Counting of colony-forming units (CFUs) on lysogeny broth (LB) medium, also indicated that bacterial abundance of TiO<sub>2</sub>-

exposed eggs was higher than that of controls eggs ( $8.5 \cdot 10^2 \pm 4.2 \cdot 10^2$  vs.  $52 \pm 23$  CFUs $\cdot$ egg $^{-1}$ ). Furthermore, without continued exposure to TiO<sub>2</sub>, this increased total microbial abundance was still present at the 5 dpf-larval stage ( $1.5 \cdot 10^4 \pm 0.6 \cdot 10^4$  vs.  $2.5 \cdot 10^3 \pm 0.5 \cdot 10^3$  CFUs $\cdot$ larva $^{-1}$ ), indicating that the impacts of TiO<sub>2</sub> on microbiota can persist across different life stages. No clear effect of exposure on microbial composition could be identified by way of 16S rRNA-based identification of the isolated bacteria (**Fig. 5**). Similarly, carbon-substrate utilization profiles neither differed between microbiota of exposed and non-exposed embryos (1 dpf), nor between microbiota of exposed and non-exposed larvae (5 dpf), as determined using EcoPlates.

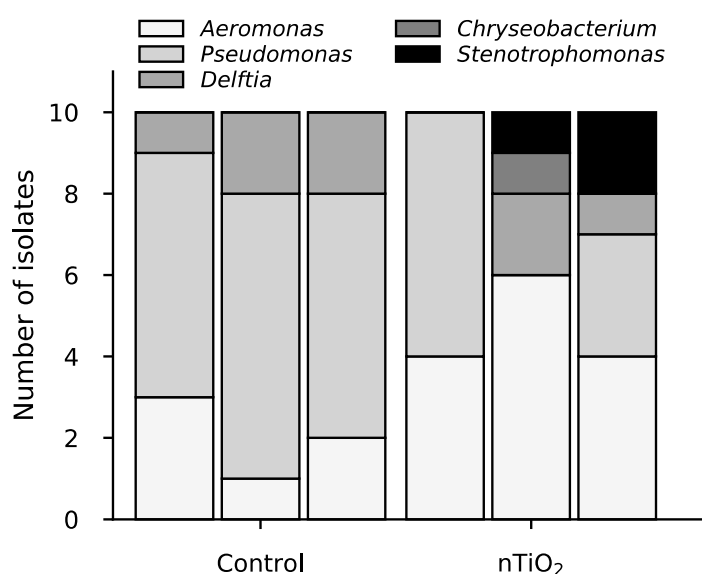


**Figure 5. Identification of bacterial isolates from control and TiO<sub>2</sub>-exposed zebrafish embryos at 1 dpf based on 16S rRNA sequence (Brinkmann et al., 2021).**

#### 2.2.2.2 Zebrafish larvae microbiota studies (UL)

The effect of host-associated microbiota on Ag NP toxicity was studied using zebrafish larvae. To this end, the sensitivity of germ-free and microbially-colonized larvae was compared in acute toxicity tests performed from 3-5 dpf. At the end of these toxicity tests, microbiota was isolated from larvae exposed to the lowest, sublethal exposure concentration ( $0.25$  mg Ag $\cdot$ L $^{-1}$ ) and from controls (no NPs), to assess the impacts of Ag NPs on host-associated microbiota.

The sensitivity of germ-free larvae to Ag NPs was much higher than that of their microbially-colonized siblings (**Fig. 6**). This revealed that colonizing microbiota can protect their host against Ag NP toxicity. At the sublethal concentration of these tests, less bacteria could be isolated on LB medium from exposed zebrafish larvae ( $0.89 \pm 0.59$  CFUs $\cdot$ larva $^{-1}$ ) than from controls ( $8.4 \cdot 10^3 \pm 3.6 \cdot 10^3$  CFUs $\cdot$ larva $^{-1}$ ). This bactericidal activity of Ag NPs also resulted in

shifts in the composition of bacterial isolates from zebrafish larvae (**Fig. 7**). Most notably, exposure to AgNP resulted in a higher abundance of *Phyllobacterium myrsinacearum* (63% vs. 30%), and the disappearance of pseudomonads (initially 30%), *Rhizobium rhizoryzae* (initially 17%), *Delftia* bacteria (initially 17%) and *Sphingomonas leidyi* (initially 7%) amongst bacterial isolates. Since little is known about the role of *P. myrsinacearum* in zebrafish larvae, the consequences thereof are still unknown.

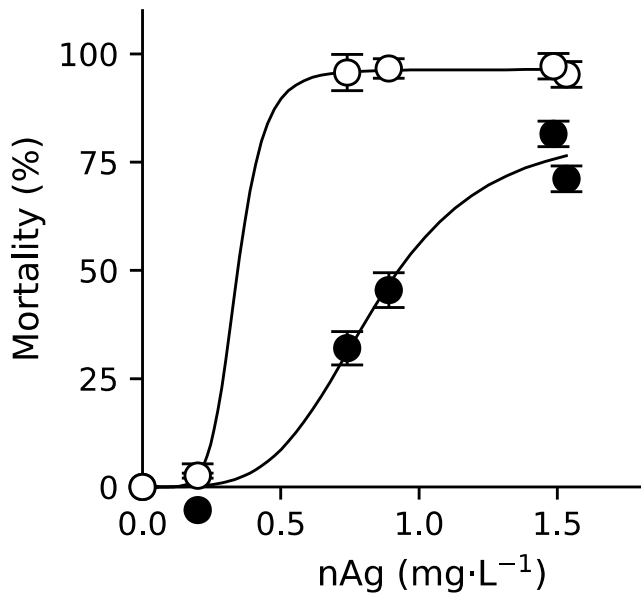


**Figure 6. Difference in sensitivity of germ-free (white circles) and microbially-colonized (black circles) zebrafish larvae (5 dpf) to acute toxicity of Ag NPs.** Particle-specific mortality, derived from response-addition calculations, and actual particulate Ag NP concentrations are depicted (published in *Nanotoxicology*; Brinkmann et al., 2020)

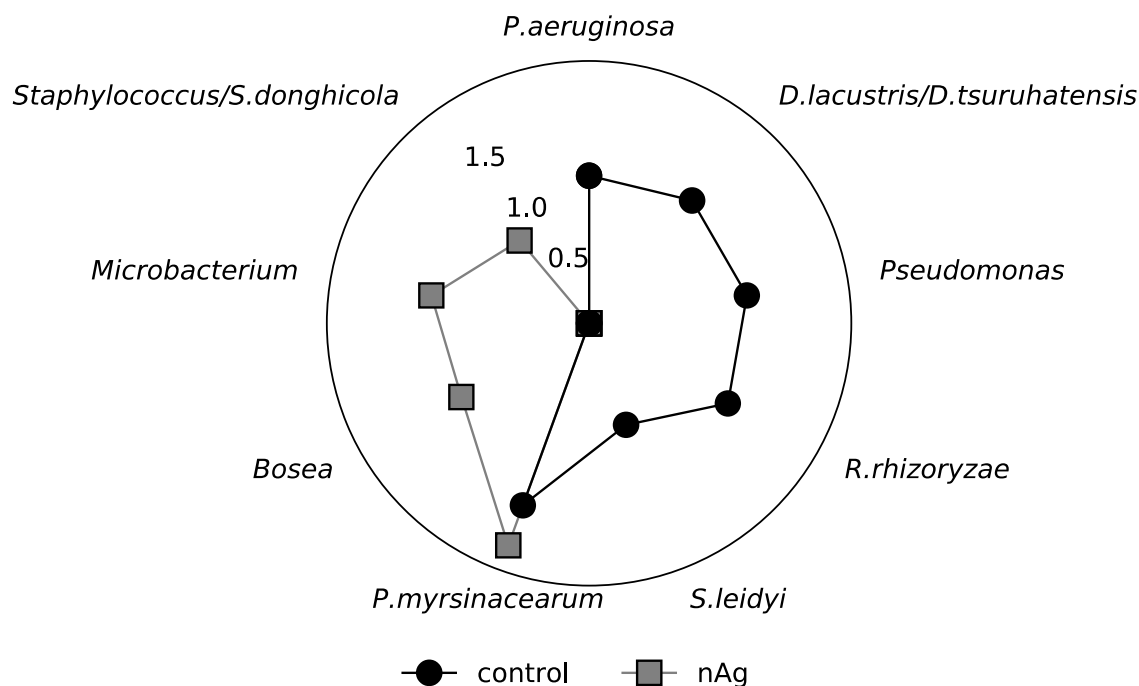


**Figure 7. Identification of bacterial isolates from control and TiO<sub>2</sub>-exposed zebrafish larvae at 5 dpf, based on 16S rRNA sequence.** Log-transformed relative abundances of bacterial isolates are depicted on the radial axes of the spider plot (published in *Nanotoxicology*; Brinkmann et al., 2020).

#### 2.2.2.3 Adult zebrafish aqueous exposure study (Literature)

In adult zebrafish, Ag NPs were found to exert sex-dependent effects on intestinal microbiota (Ma et al., 2018). Prior to exposure, male-comprised intestinal microbiota exhibited significantly higher richness (OTUs and Chao1 estimate) and diversity (Shannon's H index) than females. The relative abundance of Proteobacteria in male intestinal microbiota (65%) was higher than in that of females (36%). A small fraction of all microbiota belonged to the Proteobacteria genus *Aeromonas* (3% in males, 14% in females), which includes several pathogenic species (Fernández-Bravo and Figueras, 2020). In contrast to the Proteobacteria, the relative abundance of Fusobacteria was higher in female microbiota (53%) than in male microbiota (7%). All Fusobacteria belonged to the genus *Cetobacterium*, which includes species *Cetobacterium somerae*. This has been suggested to be an important beneficial commensal bacterium to fish for its efficient production of vitamin B12 (Tsuchiya et al., 2007).

Although aqueous exposure to Ag NPs resulted in a similar particle burden in male and female intestines (**Table 4**) and affected the intestinal somatic body index of both sexes similarly, only the relative composition of male intestinal microbiota was affected by the particles. Both the

diversity and richness of male intestinal microbiota were lower following exposure, as compared to controls. Most notably, similar to female microbiota prior to exposure, microbiota of exposed males comprised a higher relative abundance of both *Cetobacterium* (to 37-57%) and *Aeromonas* (to 3-19%) following exposure, compared to the starting point. Given the beneficial characteristics of *C. somerae*, and pathogenic potential of many aeromonads, the consequences thereof to host health merit further investigation.

### 2.2.3 Zebrafish cross-species comparison studies - Adult Zebrafish oral exposure studies (HWU)

Experiments were conducted to establish the dietary effects of CeO<sub>2</sub>-ENMs on epithelial mucosae and microbiome in adult zebrafish (*Danio rerio*). In this work adult zebrafish were exposed (14 d) to control feed, and feed containing CeO<sub>2</sub>-ENMs or bulk CeO<sub>2</sub>, each at either 500 mg or 2000 mg/kg feed. Consistent with our previous research on effects of dietary ENM exposure in adult zebrafish (Merrifield et al., 2013; Patsiou et al 2020), fish were euthanized 14 d after exposure and the intestine sampled to assess presence of cerium (analytical chemistry), evaluation of lesions in the epithelial mucosae (histopathology), and effects on the microbiome.

At the end of the 14-d exposure four fish from each feed exposure condition (control, 500 mg or 2000 mg CeO<sub>2</sub>-ENMs per kg feed) were euthanized, an incision made in the abdomen, and placed in Bouin's fixative for 24 h in preparation for histopathology. The trunk region was divided into two parts (cross section) dehydrated through an ethanol series and Histo-Clear (National Diagnostics Inc., UK), and embedded in paraffin for histological sectioning (5 µm sections). Serial transverse sections were collected from two regions of the trunk for examination of anterior and posterior portions of the intestine, and sections were stained with haematoxylin and eosin and examined by light microscopy (up to 1000X magnification). While the priority of the histological examination was the intestine, the presence of lesions in liver, trunk kidney, and spleen were also assessed.

Histopathology of fish fed control feed demonstrated normal architecture of liver, trunk kidney, and spleen consistent with adult zebrafish maintained in laboratory conditions (e.g., Patsiou et al., 2020; Henry et al., 2009). No lesions were detected in these tissues in zebrafish after ingestion of feeds containing 500 mg or 2000 mg CeO<sub>2</sub>-ENMs per kg feed. Within zebrafish fed control feed, occasional minor abrasion/erosion of the columnar epithelia of the intestinal mucosae were observed in anterior and posterior regions of the intestine, but otherwise the appearance of the brush border was normal (**Figure 8**) as observed previously with other ENMs

(Patsiou et al., 2020) and there was no evidence of inflammation or necrosis of the mucosae. Zebrafish fed feed containing CeO<sub>2</sub>-ENMs did not have any lesions in the intestine that differed from the normal appearance of intestine in control fish. Results of our histological examination of the intestine of adult zebrafish were consistent (i.e., no lesions in morphology) with our previous research of zebrafish fed feed containing ENMs in which some changes in intestinal microbiota were detected [Cu-ENMs and Ag-ENMs (Merrifield et al., 2013)] or were not detected [Pb-halide perovskite ENMs (Patsiou et al., 2020)].

In comparison, results of toxicological effects of dietary exposure to the ENMs tested are consistent across zebrafish and murine models (**Table 5**). Overall, effects of ENM exposure on the endpoints considered were minimal. Gross observations indicated that there were no adverse feeding responses [i.e., animals readily ate feeds amended with ENMs (even at relatively high exposure levels 2000 mg/kg feed)] and dietary exposure was evident by detection of feed within the intestine. There was no evidence of gross lesions within the intestine, and histopathology revealed no differences compared to unexposed controls in zebrafish. For mice there were no lesions in the intestinal tissue or effects of ENMs on DNA damage, oxidative stress or DNA repair. Incidentally, results of minimal toxicity *in vivo* are also reflected in the *in vitro* ENM exposure tests in which no cytotoxicity, DNA damage or induction of pro-inflammatory responses were observed (results reported in **Deliverables 4.1** and **4.2**).

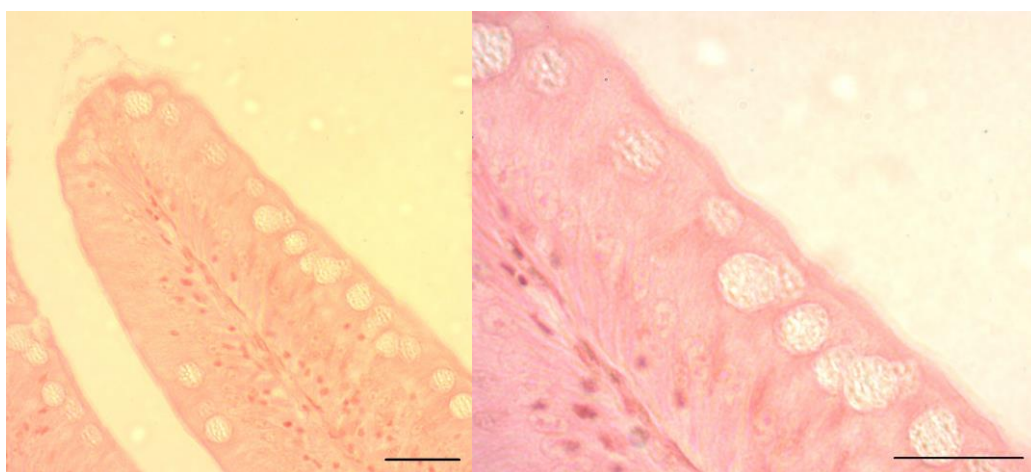


**Figure 8. Histological sections (6 μm) of zebrafish intestine (40X and 1000X Objective lens) after ingestion of feed amended with 2000 mg CeO<sub>2</sub>-ENMs /kg feed.** Occasional minor abrasion/erosion of the columnar epithelium was observed, but no lesions in tissue architecture and brush border were observed relative to the controls. Bar is 50 μm.

**Table 5. Relevant endpoint comparison between cross-species models from WPs 2, 4 and 5.**

Endpoint	Mice (WP2) [Ag-PVP, TiO <sub>2</sub> , SiO <sub>2</sub> , CeO <sub>2</sub> ]	<i>In vitro</i> (WP4) [Ag-PVP, TiO <sub>2</sub> ]	Zebrafish (WP5) [CeO <sub>2</sub> ]
<b>Toxicity</b>	Normal histology	No increase in LDH	Normal Histology
<b>Inflammation</b>	No change in Mip.2, Kc, Il1 $\beta$ , Il6, Tnf $\alpha$	No change in IL8, IL6, TNF $\alpha$	No evidence of inflammation (histopathology)
<b>DNA damage</b>	No increase detected	No increase detected	Not analysed
<b>Role of microbiome</b>	Few changes on phylum and genus levels; sex specificity	Co-incubation with BA points towards effects on ENM-induced toxicity	Not analysed

#### 2.2.4 Conclusions

Collaboration between WP2 and WP4 resulted in the generation of rodent *in vivo* microbiome transcriptome data (IUF). This data was included in **Deliverable 2.3** and was shared with WP5 (HWU, UL) to support the cross-species comparison activity and identify overlaps in responses across models to enhance the ability for extrapolation. This extrapolation would only be possible if parallel experiments were available in environmental models. Thus, IUF and HWU, liaised closely regarding the already completed rodent study to establish a possible comparable Zebrafish experimental set-up to facilitate data comparison and extrapolation. The outcome of this analysis using CeO<sub>2</sub>-ENMs was that the results of toxicological effects of dietary exposure to the ENMs tested were consistent across zebrafish and murine models.

Following comparisons between the rodent (IUF) and zebrafish (UL) microbiome data it has become clear that vertebrate responses to microbial colonization of the gut are ancient as functional genomic studies disclosed shared host responses to their compositionally distinct microbial communities and distinct microbial species that elicit conserved responses.

The use of high content analysis methods (such as membrane-based antibody arrays used here) turned out to be a promising approach to conduct *in vivo-in vitro* comparisons as well as to screen ENM effects more broadly *in vitro*. Although resource-intensive, it allows the analysis

of endpoints not routinely investigated and may generate crucial information for the necessary validation of *in vitro* models against animal or human-derived data.

### 2.3 References

Banh S, Wiens L, Sotiri E, Treberg JR (2016). Mitochondrial reactive oxygen species production by fish muscle mitochondria: Potential role in acute heat-induced oxidative stress. *Comparative Biochemistry and Physiology Part B: Biochemistry and Molecular Biology*, 191, 99–107. doi:10.1016/J.CBPPB.2015.10.001.

Binda C, Lopetuso LR, Rizzatti G, Gibiino G, Cennamo V, Gasbarrini A (2018). Actinobacteria: A relevant minority for the maintenance of gut homeostasis. *Dig Liver Dis*. 50(5):421-428.

Borycka-Kiciak K, Banasiewicz T, Rydzewska G (2017). Butyric acid - a well-known molecule revisited. *Prz Gastroenterol*. 12(2):83-89.

\* Brinkmann BW, Beijk WF, Vlieg RC, Van Noort SJT, Mejia J, Colaux JL, Lucas S, Lamers G, Peijnenburg WJGM, Vijver MG. Adsorption of titanium dioxide nanoparticles onto zebrafish eggs affects colonizing microbiota. *Aquat. Toxicol.*, 232, 105744.

\* Brinkmann BW, Koch BEV, Spaink HP, Peijnenburg WJGM, Vijver MG (2020). Colonizing microbiota protect zebrafish larvae against silver nanoparticle toxicity. *Nanotoxicology*, 14(6): 725-739.

Cossins AR, Crawford DL (2005). Fish as models for environmental genomics. *Nature Reviews Genetics*, 6(4), 324–333.

Fernández-Bravo A, Figueras MJ (2020). An update on the genus *Aeromonas*: Taxonomy, epidemiology, and pathogenicity. *Microorganisms*, 8:129.

Fuss IJ, Neurath M, Boirivant M, Klein JS, de la Motte C, Strong SA, Fiocchi C, Strober W (1996). Disparate CD4+ lamina propria (LP) lymphokine secretion profiles in inflammatory bowel disease. Crohn's disease LP cells manifest increased secretion of IFN-gamma, whereas ulcerative colitis LP cells manifest increased secretion of IL-5. *Journal of Immunology* 157 (3);1261-1270.

Henry TB, McPherson JT, Rogers ED, Heah TP, Hawkins SA, Layton AC, Sayler GS (2009). Changes in the relative expression pattern of multiple vitellogenin genes in adult male and larval zebrafish exposed to exogenous estrogens. *Comparative Biochemistry and Physiology: Part A*

*Molecular and Integrative Physiology* 154:119-126.

Ma Y, Song L, Lei Y, Jia P, Lu C, Wu J, Xi C, Strauss PR, Pei D-S (2018). Sex dependent effect of silver nanoparticles on the zebrafish gut microbiota. *Environ. Sci: Nano*, 5: 740-751.

Manke A, Wang L, Rojanasakul Y (2013). Mechanisms of nanoparticle-induced oxidative stress and toxicity. *BioMed Research International*, 2013, 942916.

Mendoza R P, Brown JM (2019). Engineered nanomaterials and oxidative stress: Current understanding and future challenges. *Current Opinion in Toxicology*, 13, 74–80.

Merrifield DL, Shaw BJ, Harper GM, Saoud IP, Davies SJ, Handy RD, Henry TB (2013). Ingestion of food containing metal nanoparticles disrupts endogenous microbiota in zebrafish with potential implications on organism health. *Environmental Pollution* 174:157-163.

\*\*Mourabit S, Fitzgerald JA, Ellis RP, Takesono A, Porteus CS, Trznadel M, Metz J, Winter MJ, Kudoh T, Tyler CR (2019). New insights into organ-specific oxidative stress mechanisms using a novel biosensor zebrafish. *Environment International*, 133, 105138.

Patsiou D, del Rio-Cubilledo C, Catarino AI, Summers S, Fahmi AM, Boyle D, Fernandes TF, Henry TB. 2020. Exposure to Pb-halide perovskite nanoparticles can deliver bioavailable Pb but does not alter endogenous gut microbiota in zebrafish. *Science of the Total Environment* 715(2020) 136941.

Rothlin CV, Leighton JA, Ghosh S (2014). Tyro3, Axl, and Mertk Receptor Signaling in Inflammatory Bowel Disease and Colitis-associated Cancer. *Inflammatory Bowel Diseases*, 20(8) 1472–1480.

Setyawati M I, Tay CY, Leong DT (2013). Effect of zinc oxide nanomaterials-induced oxidative stress on the p53 pathway. *Biomaterials*, 34(38), 10133–10142.

Singh UP, Singh NP, Murphy EA, Price RL, Fayad R, Nagarkatti M, Nagarkatti PS (2016). Chemokine and cytokine levels in inflammatory bowel disease patients. *Cytokine*. 77:44-9.

Tojo R, Suárez A, Clemente MG, de los Reyes-Gavilán CG, Margolles A, Gueimonde M, Ruas-Madiedo P (2014). Intestinal microbiota in health and disease: role of bifidobacteria in gut homeostasis. *World J Gastroenterol*. 7;20(41):15163-76.

Tsuchiya C, Sakata T, Sugita H (2007). Novel ecological niche of *Cetobacterium somerae*, an anaerobic bacterium in the intestinal tracts of freshwater fish. *Appl. Microbiol.*, 46(1): 43-48.

UniProt: a worldwide hub of protein knowledge. (2019). *Nucleic Acids Research*, 47(D1), D506–D515. doi:10.1093/nar/gky1049.

Załęski A, Banaszekiewicz A, Walkowiak J (2013). Butyric acid in irritable bowel syndrome. *Prz Gastroenterol.* 8(6):350-3.

\* References from the PATROLS project, resulting from the activity described in this deliverable.

\*\* References from the PATROLS project.

### **3. Deviations from the Workplan**

No significant deviations from the original workplan arose during the development of this deliverable. The only notable change was the contributions from partners IUF, UL and UNEXE to both the Task 4.5 activity and in the preparation of this deliverable, which was not originally foreseen in the DoA. During the Task 4.5 activity, there was very close collaboration between WP2, 4 and 5 to support the cross-species comparisons described in the DoA. Given this integrated activity across the WPs, additional partners from WP2 (IUF) and WP5 (UNEXE and UL) contributed to the generation of the present deliverable, as described further in Section 4 below.

### **4. Performance of the partners**

All partners contributed to the task as requested and fulfilled their requirements in a satisfactory time period. The report was drafted by SU with input from IUF, HWU, UL and UNEXE. In the DoA, partners IUF, UL and UNEXE were not indicated as participating in Task 4.5. However, their input to this deliverable has been critical to facilitate the linkage and close collaboration between WP2, 4 and 5. This was essential to enable the cross-species comparisons spanning rodents (WP2; IUF), human cell lines (WP4; SU, HWU, IUF) and ecological species (WP5; UL, UNEXE).

## 5. Conclusions

The Steering Board deems this deliverable to be satisfactorily fulfilled and approved for submission.

## 6. Annex

1. Molecular Initiating Events (MIEs) / Key Events (KEs), biomarkers and assays for PATROLS-relevant liver AOPs
2. Additional data to support Section 2.1.1 Mapping the molecular underpinnings for AOPs for oxidative responses to metal based ENMs in zebrafish against mammals
3. Supporting *in vitro* GIT model data following ENM exposure in the presence or absence of the microbial metabolite butyric acid

## Annex 1: Molecular Initiating Events (MIEs) / Key Events (KEs), biomarkers and assays for PATROLS-relevant liver AOPs.

Types of evidence in the below tables were coded as follows:

- A Association between *in vitro* and *in vivo* data
- B Implication in the AO (deficient or transgenic mice, inhibitors, etc)
- C Strongly associated with the AO
- D *In vivo* transcriptomics
- E Data mining
- F Other (specified)

The left side of the table (white cells) include information found in the literature that suggested a predictive potential of the marker. While the right side of the table (green cells) was completed by WP3 and 4 *in vitro* partners based on the biomarkers and advanced culture models used in PATROLS.

### 1) MIEs/KEs, biomarkers and assays for liver inflammation.

<b>Liver fibrosis</b>	Person of contact	Penny Nymark (penny.nymark@ki.se)
	KE based on:	<a href="https://aopwiki.org/aops/144">https://aopwiki.org/aops/144</a> Gerloff et al. 2016, doi.org/10.1016/j.comtox.2016.07.001
	Markers based on:	Kohonen et al. 2017, doi: 10.1038/ncomms15932 (Pathways related to the PTGS components are derived from Supplemental Data 4b. Genes for each components are available in Supplemental Data 2)

Red pathways indicate overlap with AOPwiki description of the KE.

KE that are not covered by PATROLS in vitro strategy					To be filled by partners				
KE number	KE	markers	cell type	assay	Type of evidence	markers	cell type	assay	partner
1539	<a href="#">Endocytotic lysosomal uptake</a>								
898	<a href="#">Lysosome, Disruption</a>								

209	<a href="#">Oxidative Stress, Increase</a>	<p><b>PTGS component G, H and N (in total 242 genes related to the following IPA ToxList pathways:</b> Cardiac Hypertrophy; Liver Necrosis/Cell Death; Liver Proliferation; Cardiac Fibrosis; Mechanism of Gene Regulation by Peroxisome Proliferators via PPARa; Renal Necrosis/Cell Death; Increases Liver Hyperplasia/Hyperproliferation; Primary Glomerulonephritis; Biomarker Panel (Human); RAR Activation; Hepatic Cholestasis; Cardiac Necrosis/Cell Death; VDR/RXR Activation; <b>Oxidative Stress (ICAM1, JUN, NFKB2, NFKB1)</b>; Increases Cardiac Dysfunction; Acute Renal Failure Panel (Rat); Increases Liver Damage; NRF2-mediated Oxidative Stress Response; p53 Signaling; Hepatic Stellate Cell Activation; NF-kB Signaling; Hypoxia-Inducible Factor Signaling; Aryl Hydrocarbon Receptor Signaling; Increases Heart Failure; PPARa/RXRa Activation; LXR/RXR Activation; Hepatic Fibrosis</p>	Hepatocyte (e.g. HepG2, HepRG)	transcriptomics, whole genome or reduced feature high-throughput transcriptomics of PTGS (1331 genes)	C	Oxidative Stress	HepG2 hepatocyte monoculture HepG2/Kupffer cell co-culture	RT-PCR Biorad Hepatocarcinoma Panel (AOP Genes of Interest: JUN, NFKB1, SOD, HIF-1α and MAPK)	SU
						ROS	HepG2 hepatocyte monoculture HepG2/Kupffer cell co-culture	CM-H2DCFDA - Invitrogen (Cat#C6827)	SU
						Oxidative stress response	HepG2 BAC-GFP reporters (SRXN1, HMOX1, NQO1, NRF2, KEAP1)	Confocal microscopy	Leiden
						Lipid peroxidation (TBARS)	3D human primary multicellular MT	Abcam	HWU

<p><a href="#">177</a></p>	<p><a href="#">Mitochondrial dysfunction</a></p>	<p><b>PTGS component I (in total 76 genes related to the following IPA ToxList pathways:</b> Increases Liver Damage; Renal Necrosis/Cell Death; Cardiac Hypertrophy; Hepatic Fibrosis; Cardiac Fibrosis; VDR/RXR Activation; TGF-<math>\beta</math> Signaling; Liver Proliferation; Cardiac Necrosis/Cell Death; Increases Renal Damage; Hepatic Stellate Cell Activation; Liver Necrosis/Cell Death; <b>Decreases Transmembrane Potential of Mitochondria and Mitochondrial Membrane(TGM2,IFNG,BNIP3,FGF2,MAPK9)</b>; Increases Renal Proliferation; Cell Cycle: G1/S Checkpoint Regulation; Increases Cardiac Dilation; Anti-Apoptosis; Hepatic Cholestasis; Increases Cardiac Dysfunction; Increases Glomerular Injury)</p>	<p>Hepatocyte (e.g. HepG2, HepRG)</p>	<p>transcriptomics, whole genome or reduced feature high-throughput transcriptomics of PTGS (1331 genes)</p>	<p>C</p>	<p>Mitochondrial Dysfunction</p>	<p>HepG2 hepatocyte monoculture HepG2/Kupffer cell co-culture</p>	<p>RT-PCR Biorad Hepatocarcinoma Panel (AOP Genes of Interest: IFNG and FGF2)</p>	<p>SU</p>
<p><a href="#">55</a></p>	<p><a href="#">Cell injury/death</a></p>	<p><b>PTGS component G, H, N and I (in total 299 genes related to the following IPA ToxList pathways:</b> Cardiac Hypertrophy; <b>Liver Necrosis/Cell Death (ADM,IFNG,NFKBIA,SMAD3,CDKN1A,MAPK9,PTGS2,SERPINE1)</b>; Liver Proliferation; Cardiac Fibrosis; Mechanism of Gene Regulation by Peroxisome Proliferators via PPAR<math>\alpha</math>; Renal Necrosis/Cell Death; Increases</p>	<p>Hepatocyte (e.g. HepG2, HepRG)</p>	<p>transcriptomics, whole genome or reduced feature high-throughput transcriptomics of PTGS (1331 genes)</p>	<p>C</p>	<p>Caspase 3/7 assay</p>	<p>3D human primary multicellular MT</p>	<p>Promega</p>	<p>HWU</p>
						<p>Cell Death</p>	<p>HepG2 hepatocyte monoculture HepG2/Kupffer cell co-culture</p>	<p>RT-PCR Biorad Hepatocarcinoma Panel (AOP Genes of Interest: IFNG, CDKN1A and PTGS2)</p>	<p>SU</p>
						<p>Cell Death/Cytotoxicity</p>	<p>HepG2 hepatocyte monoculture HepG2/Kupffer cell co-culture</p>	<p>Trypan Blue exclusion (Sigma - T8154)</p>	<p>SU</p>

		<p>Liver Hyperplasia/Hyperproliferation;                  Primary Glomerulonephritis;                  Biomarker Panel (Human); RAR                  Activation; Hepatic Cholestasis;                  Cardiac Necrosis/Cell Death; VDR/RXR                  Activation; Oxidative Stress; Increases                  Cardiac Dysfunction; Acute Renal                  Failure Panel (Rat); Increases Liver                  Damage; NRF2-mediated Oxidative                  Stress Response; p53 Signaling;                  Hepatic Stellate Cell Activation; NF-kB                  Signaling; Hypoxia-Inducible Factor                  Signaling; Aryl Hydrocarbon Receptor                  Signaling; Increases Heart Failure;                  PPARa/RXRa Activation; LXR/RXR                  Activation; Hepatic Fibrosis; TGF-b                  Signaling; Increases Renal Damage;                  Decreases Transmembrane Potential                  of Mitochondria and Mitochondrial                  Membrane; Increases Renal                  Proliferation; Cell Cycle: G1/S;                  Checkpoint Regulation; Increases                  Cardiac Dilation; Anti-Apoptosis;                  Increases Glomerular Injury</p>				<p>Necrosis/                  apoptosis</p>	<p>HepG2</p>	<p>Propidium iodide /                  AnnexinV staining                  with Confocal                  microscopy</p>	<p>Leiden</p>
						<p>Adenylate                  kinase                  AND                  live/dead                  staining                  AND                  histology</p>	<p>3D human                  primary                  multicellular MT</p>	<p>Lonza AND abcam                  AND NA</p>	<p>HWU</p>

87	<a href="#">Cytokine, Release</a>					IL-8, IL-6 & TNF-α	HepG2 hepatocyte monoculture HepG2/Kupffer cell co-culture	R&D Systems (Cat#DY208) R&D Systems (Cat#DY206) R&D Systems (Cat#DY210)	SU
						IL1B, IL8, IL10, IFN-γ, TNF, IL6	3D human primary multicellular MT	Biotechne flex sets	HWU
901	<a href="#">Inflammatory cells, Infiltration</a>								
902	<a href="#">Liver, Inflammation</a>	<b>PTGS component G and N* (in total 162 genes related to the following IPA ToxList pathways:</b> Cardiac Hypertrophy; Liver Necrosis/Cell Death; Liver Proliferation; Cardiac Fibrosis; Mechanism of Gene Regulation by Peroxisome Proliferators via PPARα; Renal Necrosis/Cell Death; Increases Liver Hyperplasia/Hyperproliferation; Primary Glomerulonephritis;	Hepatocyte (e.g. HepG2, HepRG)	transcriptomics, whole genome or reduced feature high-throughput transcriptomics of PTGS (1331 genes)	C	Liver Inflammation	HepG2 hepatocyte monoculture HepG2/Kupffer cell co-culture	RT-PCR Biorad Hepatocarcinoma Panel (AOP Genes of Interest: TNFAIP3, IL1B and NFKB1)	SU
						IL1B, IL8, IL10, IFN-γ, TNF, IL6	3D human primary multicellular MT	Biotechne flex sets	HWU

		Biomarker Panel (Human); RAR Activation; Hepatic Cholestasis; Cardiac Necrosis/Cell Death; VDR/RXR Activation; Oxidative Stress; Increases Cardiac Dysfunction; Acute Renal Failure Panel (Rat); Increases Liver Damage; NRF2-mediated Oxidative; Stress Response; p53 Signaling; Hepatic Stellate Cell Activation; <b>NF-kB Signaling(TNIP1,NFKBIA,NFKBIE,RELB, TNFAIP3,IL1B,NFKB2,NFKB1);</b> Hypoxia-Inducible Factor Signaling; Aryl Hydrocarbon Receptor Signaling; Increases Heart Failure; PPARa/RXRa Activation; Hepatic Fibrosis; LXR/RXR Activation)				NFkB signaling	HepG2 BAC-GFP reporters for NFkB signaling (ICAM1, A20, RelA)	Confocal microscopy	Leiden
--	--	--	--	--	--	----------------	---	---------------------	--------

\*strongly related to the probability of the final AO happening in vivo

2) MIEs/KEs, biomarkers and assays for liver fibrosis.

**Liver fibrosis** Person of contact Penny Nymark (penny.nymark@ki.se)

KE based on: <https://aopwiki.org/aops/144>  
Gerloff et al. 2016, doi.org/10.1016/j.comtox.2016.07.001

markers based on: Kohonen et al. 2017, doi: 10.1038/ncomms15932.

(Pathways related to the PTGS components are derived from Supplemental Data 4b. Genes for each components are available in Supplemental Data 2)

Red pathways indicate overlap with AOPwiki description of the KE.

KE that are not covered by PATROLS in vitro strategy

KE number	KE	markers	cell type	assay	Type of evidence
<a href="#">1539</a>	<a href="#">Endocytotic lysosomal uptake</a>				
<a href="#">898</a>	<a href="#">Disruption, Lysosome</a>				
<a href="#">177</a>	<a href="#">N/A, Mitochondrial dysfunction 1</a>	<b>PTGS component I (in total 76 genes related to the following IPA ToxList pathways:</b> Increases Liver Damage; Renal Necrosis/Cell Death; Cardiac Hypertrophy; Hepatic Fibrosis; Cardiac Fibrosis; VDR/RXR Activation; TGF-b Signaling; Liver Proliferation; Cardiac Necrosis/Cell Death; Increases Renal Damage; Hepatic Stellate Cell Activation; Liver Necrosis/Cell Death; <b>Decreases Transmembrane Potential of Mitochondria and Mitochondrial Membrane(TGM2,IFNG,BNIP3,FGF2,MAPK9)</b> ; Increases Renal Proliferation; Cell Cycle: G1/S	Hepatocyte (e.g. HepG2, HepRG)	transcriptomics, whole genome or reduced feature high-throughput transcriptomics of PTGS (1331 genes)	C

To be filled by partners			
markers	cell type	assay	partner
Mitochondrial Dysfunction	HepG2 hepatocyte monoculture HepG2/Kupffer cell co-culture	RT-PCR Biorad Hepatocarcinoma Panel (AOP Genes of Interest: IFNG and FGF2)	SU

		Checkpoint Regulation; Increases; Cardiac Dilation; Anti-Apoptosis; Hepatic Cholestasis; Increases Cardiac Dysfunction; Increases Glomerular Injury				Caspase 3/7 assay	HepG2	Caspase-3/7-glo assay	Misvik
55	<a href="#">N/A, Cell injury/death</a>	<b>PTGS component G, H, N and I (in total 299 genes related to the following IPA ToxList pathways:</b> Cardiac Hypertrophy; <b>Liver Necrosis/Cell Death (CXCL3, TNIP1, JUN, NFKB1A, IER3, CEBP B, CFLAR, RXRA, NFKB1)</b> ; Liver Proliferation; Cardiac Fibrosis; Mechanism of Gene Regulation by; Peroxisome Proliferators via PPARa; Renal Necrosis/Cell Death; Increases Liver Hyperplasia/Hyperproliferation; Primary Glomerulonephritis; Biomarker Panel (Human); RAR Activation; Hepatic Cholestasis; Cardiac Necrosis/Cell Death; VDR/RXR Activation; Oxidative Stress; Increases Cardiac Dysfunction; Acute Renal Failure Panel (Rat); Increases Liver Damage; NRF2-mediated Oxidative	Hepatocyte (e.g. HepG2, HepRG)	transcriptomics, whole genome or reduced feature high-throughput transcriptomics of PTGS (1331 genes)	C	Cell Death	HepG2 hepatocyte monoculture HepG2/Kupffer cell co-culture	RT-PCR Biorad Hepatocarcinoma Panel (AOP Genes of Interest: JUN, RXRA and NFKB1)	SU
						Cell Death/Cytotoxicity	HepG2 hepatocyte monoculture HepG2/Kupffer cell co-culture	Trypan Blue exclusion (Sigma - T8154)	SU
						Necrosis/apoptosis	HepG2	Propidium iodide / AnnexinV staining with Confocal microscopy	Leiden
						Cell viability	HepG2	CellTiter-Glo assay	Misvik
						Cell Number	HepG2	Dapi staining	Misvik

		Stress Response; p53 Signaling; Hepatic Stellate Cell Activation; NF-kB Signaling; Hypoxia-Inducible Factor Signaling; Aryl Hydrocarbon Receptor Signaling; Increases Heart Failure; PPARa/RXRa Activation; LXR/RXR Activation; Hepatic Fibrosis; TGF-b Signaling; Increases Renal Damage; Decreases Transmembrane Potential of Mitochondria and Mitochondrial Membrane; Increases Renal Proliferation; Cell Cycle: G1/S Checkpoint Regulation; Increases Cardiac Dilatation; Anti-Apoptosis; Increases Glomerular Injury				Nucleic acid oxidative stress	HepG2	8OHG staining	Misvik
						DNA damage	HepG2	gamma-H2AX staining	Misvik
						Apoptosis	HepG2	Caspase-3/7-glo assay	Misvik
<a href="#">1493</a>	<a href="#">Increased Pro-inflammatory mediators</a>	<b>PTGS component G and N (in total 162 genes related to the following IPA ToxList pathways:</b> Cardiac Hypertrophy; Liver Necrosis/Cell Death; Liver Proliferation; Cardiac Fibrosis; Mechanism of Gene Regulation by Peroxisome Proliferators via PPARa; Renal Necrosis/Cell Death; Increases Liver Hyperplasia/Hyperproliferation; Primary Glomerulonephritis; Biomarker Panel (Human); RAR Activation; Hepatic Cholestasis; Cardiac Necrosis/Cell Death; VDR/RXR Activation; Oxidative Stress; Increases Cardiac Dysfunction; Acute Renal Failure Panel (Rat); Increases Liver	Hepatocyte (e.g. HepG2, HepRG)	transcriptomics, whole genome or reduced feature high-throughput transcriptomics of PTGS (1331 genes)	C	Liver Inflammation	HepG2 hepatocyte monoculture HepG2/Kupffer cell co-culture	RT-PCR Biorad Hepatocarcinoma Panel (AOP Genes of Interest: TNFAIP3, IL1B, IL8 and NFKB1)	SU
						IL-8, IL-6 & TNF-α	HepG2 hepatocyte monoculture HepG2/Kupffer cell co-culture	R&D Systems (Cat#DY208) R&D Systems (Cat#DY206) R&D Systems (Cat#DY210)	SU

		Damage; NRF2-mediated Oxidative Stress Response; p53 Signaling; Hepatic Stellate Cell Activation; <b>NF-kB Signaling(TNIP1,NFKBIA,NFKBIE,RELB ,TNFAIP3,IL1B,NFKB2,NFKB1)</b> ; Hypoxia-Inducible Factor Signaling; Aryl Hydrocarbon Receptor Signaling; Increases Heart Failure; PPARa/RXRa Activation; Hepatic Fibrosis; LXR/RXR Activation				NFkB signaling	HepG2 BAC-GFP reporters for NFkB signaling (ICAM1, A20, RelA)	Confocal microscopy	Leiden
1494	<a href="#">Leukocyte recruitment/activation</a>								
265	<a href="#">Activation, Stellate cells</a>	<b>PTGS component G, N and I (in total 226 genes related to the following IPA ToxList pathways:</b> Cardiac Hypertrophy; Liver Necrosis/Cell Death; Liver Proliferation; Cardiac Fibrosis; Mechanism of Gene Regulation by Peroxisome Proliferators via PPARa; Renal Necrosis/Cell Death; Increases Liver Hyperplasia/Hyperproliferation; Primary Glomerulonephritis; Biomarker Panel (Human); RAR Activation; Hepatic Cholestasis; Cardiac Necrosis/Cell Death; VDR/RXR Activation; Oxidative Stress; Increases Cardiac Dysfunction; Acute Renal Failure Panel (Rat); Increases Liver Damage; NRF2-mediated Oxidative	Hepatocyte (e.g. HepG2, HepRG)	transcriptomics, whole genome or reduced feature high-throughput transcriptomics of PTGS (1331 genes)	C	Stellate Cell Activation	HepG2 hepatocyte monoculture HepG2/Kupffer cell co-culture	RT-PCR Biorad Hepatocarcinoma Panel (AOP Genes of Interest: IL8 and NFKB1)	SU
						Stellate activation	3D human primary multicellular MT containing stellate cells	alpha-SMA ELISA, LOX activity, Col1A1 expression (qPCR), p3np (procollagen III N-terminal peptide) ELISA	HWU / Insphero

		<p>Stress Response; p53 Signaling; <b>Hepatic Stellate Cell Activation (IL8,PDGFA,NFKB2,NFKB1)</b>; NF-kB Signaling; Hypoxia-Inducible Factor Signaling; Aryl Hydrocarbon Receptor Signaling; Increases Heart Failure; PPARa/RXRa Activation; Hepatic Fibrosis; <b>TGF-b Signaling (SMAD3,TGFB2,MAPK9,MAP2K3,SMURF2,SERPINE1)</b>; Increases Renal Damage; Decreases Transmembrane Potential of Mitochondria and Mitochondrial Membrane; Increases Renal Proliferation; Cell Cycle: G1/S Checkpoint Regulation; Increases Cardiac Dilatation; Anti-Apoptosis; Increases Glomerular Injury; LXR/RXR Activation</p>				<p>Stellate activation and Pathology</p>	<p>3D human primary multicellular MT containg stellate cells</p>	<p>Histology - Trichrome Masson staining, Siriusred staining with dark field microscopy; collagen 1 and 4 staining</p>	<p>HWU / Insphero</p>
68	<p><a href="#">Accumulation, Collagen</a></p>								

344	<a href="#">N/A, Liver fibrosis</a>	<p><b>PTGS component N and I* (in total 106 genes related to the following IPA ToxList pathways:</b> Increases Liver Damage; Renal Necrosis/Cell Death; Cardiac Hypertrophy; <b>Hepatic Fibrosis (IL8,ICAM1,PDGFA,IL1B,CXCL2)</b>; Cardiac Fibrosis; VDR/RXR Activation; TGF-b Signaling; Liver Proliferation; Cardiac Necrosis/Cell Death; Increases Renal Damage; Hepatic Stellate Cell Activation; Liver Necrosis/Cell Death; Decreases Transmembrane Potential of Mitochondria and Mitochondrial Membrane; Increases Renal Proliferation; Cell Cycle: G1/S Checkpoint Regulation; Increases Cardiac Dilatation; Anti-Apoptosis; Hepatic Cholestasis; Increases Cardiac Dysfunction; Increases Glomerular Injury; PPARa/RXRa Activation; Mechanism of Gene Regulation by; Peroxisome Proliferators via PPARa; NF-kB Signaling; Aryl Hydrocarbon Receptor Signaling; Oxidative Stress; LXR/RXR Activation; RAR Activation</p>	Hepatocyte (e.g. HepG2, HepRG)	transcriptomics, whole genome or reduced feature high-throughput transcriptomics of PTGS (1331 genes)	C	Fibrosis	HepG2 hepatocyte monoculture HepG2/Kupffer cell co-culture	RT-PCR Biorad Hepatocarcinoma Panel (AOP Genes of Interest: IL8 and IL1B)	SU
-----	-------------------------------------	---	--------------------------------	---	---	----------	---	---	----

\*strongly related to the probability of the final AO happening *in vivo*

### 3) MIEs/KEs, biomarkers and assays for liver cancer.

**Liver cancer** Person of contact Ulla Birgitte Vogel (UBV@nfa.dk)

KE based on: <https://aopwiki.org/events/378>

PMID: 29298701 Modrzynska et al, Part Fibre Toxicol. 2018 Jan 3;15(1):2. doi: 10.1186/s12989-017-0238-9.

Markers based on: PMID: 18618583; Jacobsen et al, Environ Mol Mutagen. 2008 Jul;49(6):476-87. doi: 10.1002/em.20406

#### KE that are not covered by PATROLS in vitro strategy

KE number	KE	markers	cell type	assay	Type of evidence
KE249, KE257, KE1115, KE1364	MIE: particle surface dependent ROS generation				
<a href="#">1608</a>	<a href="#">Oxidative DNA damage</a>	oxidative DNA damage/DNA adducts/DNA strand breaks in liver tissue	liver cells	oxidative DNA damage/DNA adducts/comet assay/micronucleus assay	B

#### To be filled by partners

markers	cell type	assay	partner
DNA damage, Genotoxicity	HepG2 monoculture HepG2/Kupffer cell co-culture	Cytokinesis block micronucleus assay	SU
DNA damage response	HepG2 BAC-GFP reporters for DNA damage response (P21, BTG2, MDM2, P53)	Confocal microscopy	Leiden
Oxidative DNA damage	3D human primary multicellular MT	FPG modified Comet assay	HWU
Oxidative DNA damage	HepG2 monoculture	8OHG staining	Misvik

						DNA strand breaks	HepG2 monoculture	gamma-H2AX staining	Misvik
<a href="#">185</a> <a href="#">376</a>	Increased mutations	Mutations	liver cells	in vitro assay of mutation: OECD TG 488: Transgenic Rodent Somatic and Germ Cell Gene Mutation Assays	A, B, C				
<a href="#">378</a>	<a href="#">Tumorigenesis, Hepatocellular carcinoma</a>								

**Annex 2: Additional data to support Section 2.1.1 Mapping the molecular underpinnings for AOPs for oxidative responses to metal based ENMs in zebrafish against mammals**

Supplementary Table 1: Genes shared across zebrafish and mammals involved in oxidative stress response in the liver

Entry	Entry name	Status	Protein names	Gene names	Organism
Q5T6L4	Q5T6L4_HUMAN	unreviewed	Argininosuccinate synthase 1 isoform 1 (Argininosuccinate synthetase, isoform CRA_a) (Epididymis secretory sperm binding protein) (cDNA, FLJ96050, highly similar to Homo sapiens argininosuccinate synthetase (ASS), transcript variant1, mRNA)	ASS ASS1 HCG_31245	Homo sapiens (Human)
P00966	ASSY_HUMAN	reviewed	Argininosuccinate synthase (EC 6.3.4.5) (Citrulline--aspartate ligase)	ASS1 ASS	Homo sapiens (Human)
Q9BYV7	BCDO2_HUMAN	reviewed	Beta,beta-carotene 9',10'-oxygenase (EC 1.13.11.71) (B-diox-II) (Beta-carotene dioxygenase 2)	BCO2 BCDO2	Homo sapiens (Human)
Q8WWM9	CYGB_HUMAN	reviewed	Cytoglobin (Histoglobin) (HGb) (Stellate cell activation-associated protein)	CYGB STAP	Homo sapiens (Human)
Q575S8	CYGB2_DANRE	reviewed	Cytoglobin-2	CYGB2 CYGB-2	Danio rerio (Zebrafish) (Brachydanio rerio)
Q575S8	CYGB2_DANRE	reviewed	Cytoglobin-2	CYGB2 CYGB-2	Danio rerio (Zebrafish) (Brachydanio rerio)
F1R3E6	F1R3E6_DANRE	unreviewed	Forkhead box O4	FOXO4	Danio rerio (Zebrafish) (Brachydanio rerio)
P98177	FOXO4_HUMAN	reviewed	Forkhead box protein O4 (Fork head domain transcription factor AFX1)	FOXO4 AFX AFX1 MLLT7	Homo sapiens (Human)
Q5XJ42	Q5XJ42_DANRE	unreviewed	Glrx protein (Glutaredoxin (Thioltransferase))	GLRX	Danio rerio (Zebrafish) (Brachydanio rerio)
Q9P1N5	Q9P1N5_HUMAN	unreviewed	Glutaredoxin 5 homolog (S. cerevisiae), isoform CRA_a (PRO1238)	GLRX5 HCG_24440	Homo sapiens (Human)
P35754	GLRX1_HUMAN	reviewed	Glutaredoxin-1 (Thioltransferase-1) (TTase-1)	GLRX GRX	Homo sapiens (Human)
Q6PBM1	GLRX5_DANRE	reviewed	Glutaredoxin-related protein 5, mitochondrial (Monothiol glutaredoxin-5)	GLRX5 GRX5 SHIRAZ Sl:CH211-121D13.1	Danio rerio (Zebrafish) (Brachydanio rerio)
AoA087WT12	AoA087WT12_HUMAN	unreviewed	Glutathione peroxidase	GPX4	Homo sapiens (Human)
AoA087WTS0	AoA087WTS0_HUMAN	unreviewed	Glutathione peroxidase	GPX2	Homo sapiens (Human)
AoA087WUQ6	AoA087WUQ6_HUMAN	unreviewed	Glutathione peroxidase	GPX1	Homo sapiens (Human)
AoA087X2l2	AoA087X2l2_HUMAN	unreviewed	Glutathione peroxidase	GPX4	Homo sapiens (Human)
F1R5F7	F1R5F7_DANRE	unreviewed	Glutathione peroxidase	GPX3	Danio rerio (Zebrafish) (Brachydanio rerio)
G3V4J6	G3V4J6_HUMAN	unreviewed	Glutathione peroxidase	GPX2	Homo sapiens (Human)
G3V323	G3V323_HUMAN	unreviewed	Glutathione peroxidase	GPX2	Homo sapiens (Human)
K7EJ20	K7EJ20_HUMAN	unreviewed	Glutathione peroxidase	GPX4	Homo sapiens (Human)
K7ENB4	K7ENB4_HUMAN	unreviewed	Glutathione peroxidase	GPX4	Homo sapiens (Human)
Q5XJ48	Q5XJ48_DANRE	unreviewed	Glutathione peroxidase	GPX1A GPX1	Danio rerio (Zebrafish) (Brachydanio rerio)
Q5XJ48	Q5XJ48_DANRE	unreviewed	Glutathione peroxidase	GPX1A GPX1	Danio rerio (Zebrafish) (Brachydanio rerio)

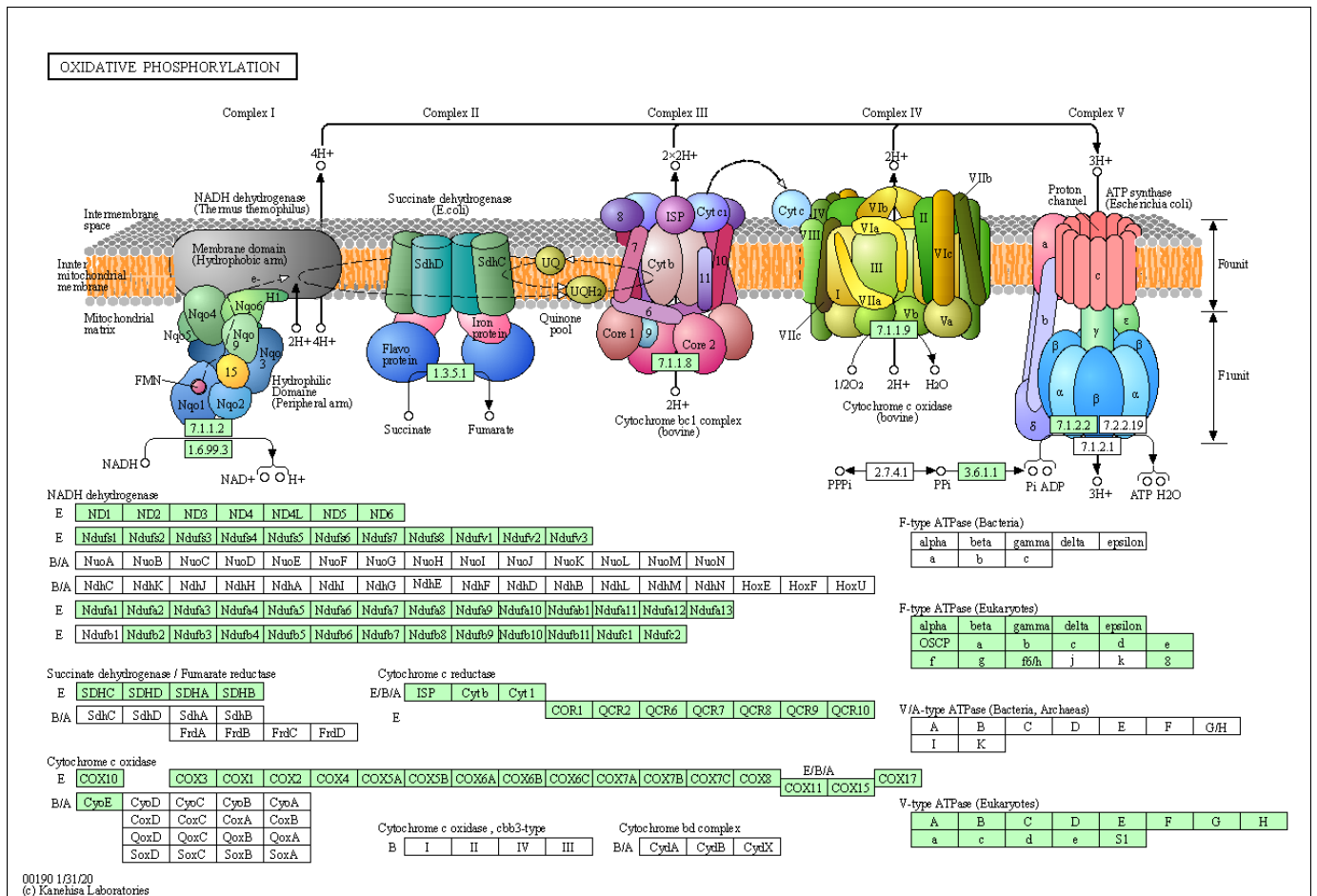
Q6DHK6	Q6DHK6_DANRE	unreviewed	Glutathione peroxidase	GPX4A	Danio rerio (Zebrafish) (Brachydanio rerio)
K7EKX7	K7EKX7_HUMAN	unreviewed	Glutathione peroxidase (Fragment)	GPX4	Homo sapiens (Human)
K7ERP4	K7ERP4_HUMAN	unreviewed	Glutathione peroxidase (Fragment)	GPX4	Homo sapiens (Human)
R4GNE4	R4GNE4_HUMAN	unreviewed	Glutathione peroxidase (Fragment)	GPX4	Homo sapiens (Human)
AoA2R8Y6B6	AoA2R8Y6B6_HUMAN	unreviewed	Glutathione peroxidase 1	GPX1	Homo sapiens (Human)
P07203	GPX1_HUMAN	reviewed	Glutathione peroxidase 1 (GPX-1) (GSHPx-1) (EC 1.11.1.9) (Cellular glutathione peroxidase)	GPX1	Homo sapiens (Human)
P18283	GPX2_HUMAN	reviewed	Glutathione peroxidase 2 (GPX-2) (GSHPx-2) (EC 1.11.1.9) (Gastrointestinal glutathione peroxidase) (Glutathione peroxidase-gastrointestinal) (GPX-GI) (GSHPx-GI) (Glutathione peroxidase-related protein 2) (GPRP-2)	GPX2	Homo sapiens (Human)
P22352	GPX3_HUMAN	reviewed	Glutathione peroxidase 3 (GPX-3) (GSHPx-3) (EC 1.11.1.9) (Extracellular glutathione peroxidase) (Plasma glutathione peroxidase) (GPx-P) (GSHPx-P)	GPX3 GPXP	Homo sapiens (Human)
AoA087WT44	AoA087WT44_HUMAN	unreviewed	Heme oxygenase 2	HMOX2	Homo sapiens (Human)
I3L1F5	I3L1F5_HUMAN	unreviewed	Heme oxygenase 2 (Fragment)	HMOX2	Homo sapiens (Human)
I3L1Y2	I3L1Y2_HUMAN	unreviewed	Heme oxygenase 2 (Fragment)	HMOX2	Homo sapiens (Human)
P30519	HMOX2_HUMAN	reviewed	Heme oxygenase 2 (HO-2) (EC 1.14.14.18)	HMOX2 HO2	Homo sapiens (Human)
Q1MT52	Q1MT52_DANRE	unreviewed	Heme oxygenase 2a (Fragment)	HMOX2A	Danio rerio (Zebrafish) (Brachydanio rerio)
A7MD59	A7MD59_DANRE	unreviewed	Heme oxygenase (EC 1.14.14.18)	HMOX2A SI:DKEY-44G23.7	Danio rerio (Zebrafish) (Brachydanio rerio)
AoA0J9YWK4	AoA0J9YWK4_HUMAN	unreviewed	Hemoglobin subunit beta	HBB	Homo sapiens (Human)
AoA2R8Y7R2	AoA2R8Y7R2_HUMAN	unreviewed	Hemoglobin subunit beta	HBB	Homo sapiens (Human)
P68871	HBB_HUMAN	reviewed	Hemoglobin subunit beta (Beta-globin) (Hemoglobin beta chain) [Cleaved into: LVV-hemorphin-7; Spinorphin]	HBB	Homo sapiens (Human)
F8W6P5	F8W6P5_HUMAN	unreviewed	Hemoglobin subunit beta (Fragment)	HBB	Homo sapiens (Human)
Q802G6	MSB1A_DANRE	reviewed	Methionine-R-sulfoxide reductase B1-A (MsrB) (MsrB1-A) (EC 1.8.4.12) (EC 1.8.4.14) (Selenoprotein X-A) (SePR) (SelX-A)	MSRB1 SEPX1 SEPX1A	Danio rerio (Zebrafish) (Brachydanio rerio)
Q9Y3D2	MSRB2_HUMAN	reviewed	Methionine-R-sulfoxide reductase B2, mitochondrial (MsrB2) (EC 1.8.4.12) (EC 1.8.4.14)	MSRB2 CBS-1 MSRB CGI-131	Homo sapiens (Human)
P28482	MK01_HUMAN	reviewed	Mitogen-activated protein kinase 1 (MAP kinase 1) (MAPK 1) (EC 2.7.11.24) (ERT1) (Extracellular signal-regulated kinase 2) (ERK-2) (MAP kinase isoform p42) (p42-MAPK) (Mitogen-activated protein kinase 2) (MAP kinase 2) (MAPK 2)	MAPK1 ERK2 PRKM1 PRKM2	Homo sapiens (Human)
P27361	MK03_HUMAN	reviewed	Mitogen-activated protein kinase 3 (MAP kinase 3) (MAPK 3) (EC 2.7.11.24) (ERT2) (Extracellular signal-regulated kinase 1) (ERK-1) (Insulin-stimulated MAP2 kinase) (MAP kinase isoform p44) (p44-MAPK) (Microtubule-associated protein 2 kinase) (p44-ERK1)	MAPK3 ERK1 PRKM3	Homo sapiens (Human)
Q13164	MK07_HUMAN	reviewed	Mitogen-activated protein kinase 7 (MAP kinase 7) (MAPK 7) (EC 2.7.11.24) (Big MAP kinase 1) (BMK-1) (Extracellular signal-regulated kinase 5) (ERK-5)	MAPK7 BMK1 ERK5 PRKM7	Homo sapiens (Human)
AoA0R4IJM3	AoA0R4IJM3_DANRE	unreviewed	Mitogen-activated protein kinase 10 (Fragment)	MAPK10	Danio rerio (Zebrafish) (Brachydanio rerio)
AoA0R4IN30	AoA0R4IN30_DANRE	unreviewed	Mitogen-activated protein kinase 10 (Fragment)	MAPK10	Danio rerio (Zebrafish) (Brachydanio rerio)
Q15759	MK11_HUMAN	reviewed	Mitogen-activated protein kinase 11 (MAP kinase 11) (MAPK 11) (EC 2.7.11.24) (Mitogen-activated protein kinase p38 beta) (MAP kinase p38 beta)	MAPK11 PRKM11 SAPK2 SAPK2B	Homo sapiens (Human)

			(p38b) (Stress-activated protein kinase 2b) (SAPK2b) (p38-2)		
E7EX54	E7EX54_HUMAN	unreviewed	Mitogen-activated protein kinase 14 (Fragment)	MAPK14	Homo sapiens (Human)
Q16539	MK14_HUMAN	reviewed	Mitogen-activated protein kinase 14 (MAP kinase 14) (MAPK 14) (EC 2.7.11.24) (Cytokine suppressive anti-inflammatory drug-binding protein) (CSAID-binding protein) (CSBP) (MAP kinase MXI2) (MAX-interacting protein 2) (Mitogen-activated protein kinase p38 alpha) (MAP kinase p38 alpha) (Stress-activated protein kinase 2a) (SAPK2a)	MAPK14 CSBP CSBP1 CSBP2 CSPB1 MXI2 SAPK2A	Homo sapiens (Human)
AoAoR4I9H8	AoAoR4I9H8_DANRE	unreviewed	Mitogen-activated protein kinase (EC 2.7.11.24)	MAPK10	Danio rerio (Zebrafish) (Brachydanio rerio)
AoAoR4IB91	AoAoR4IB91_DANRE	unreviewed	Mitogen-activated protein kinase (EC 2.7.11.24)	MAPK10	Danio rerio (Zebrafish) (Brachydanio rerio)
AoAoR4IKK9	AoAoR4IKK9_DANRE	unreviewed	Mitogen-activated protein kinase (EC 2.7.11.24)	MAPK10	Danio rerio (Zebrafish) (Brachydanio rerio)
A4QP40	A4QP40_DANRE	unreviewed	Mitogen-activated protein kinase (EC 2.7.11.24)	MAPK10	Danio rerio (Zebrafish) (Brachydanio rerio)
B4EoK5	B4EoK5_HUMAN	unreviewed	Mitogen-activated protein kinase (EC 2.7.11.24)	MAPK14	Homo sapiens (Human)
Q32LVo	Q32LVo_DANRE	unreviewed	Mitogen-activated protein kinase (EC 2.7.11.24)	MAPK10	Danio rerio (Zebrafish) (Brachydanio rerio)
E7F683	E7F683_DANRE	unreviewed	Mitogen-activated protein kinase kinase kinase 2	MAP3K2	Danio rerio (Zebrafish) (Brachydanio rerio)
Q9Y2U5	M3K2_HUMAN	reviewed	Mitogen-activated protein kinase kinase kinase 2 (EC 2.7.11.25) (MAPK/ERK kinase kinase 2) (MEK kinase 2) (MEKK 2)	MAP3K2 MAPKKK2 MEKK2	Homo sapiens (Human)
Q9Y6R4	M3K4_HUMAN	reviewed	Mitogen-activated protein kinase kinase kinase 4 (EC 2.7.11.25) (MAP three kinase 1) (MAPK/ERK kinase kinase 4) (MEK kinase 4) (MEKK 4)	MAP3K4 KIAA0213 MAPKKK4 MEKK4 MTK1	Homo sapiens (Human)
Q99683	M3K5_HUMAN	reviewed	Mitogen-activated protein kinase kinase kinase 5 (EC 2.7.11.25) (Apoptosis signal-regulating kinase 1) (ASK-1) (MAPK/ERK kinase kinase 5) (MEK kinase 5) (MEKK 5)	MAP3K5 ASK1 MAPKKK5 MEKK5	Homo sapiens (Human)
Q9UG54	Q9UG54_HUMAN	unreviewed	Mitogen-activated protein kinase kinase kinase 7	MAP3K7 DKFZP586F0420	Homo sapiens (Human)
O43318	M3K7_HUMAN	reviewed	Mitogen-activated protein kinase kinase kinase 7 (EC 2.7.11.25) (Transforming growth factor-beta-activated kinase 1) (TGF-beta-activated kinase 1)	MAP3K7 TAK1	Homo sapiens (Human)
P41279	M3K8_HUMAN	reviewed	Mitogen-activated protein kinase kinase kinase 8 (EC 2.7.11.25) (Cancer Osaka thyroid oncogene) (Proto-oncogene c-Cot) (Serine/threonine-protein kinase cot) (Tumor progression locus 2) (TPL-2)	MAP3K8 COT ESTF	Homo sapiens (Human)
Q5T853	Q5T853_HUMAN	unreviewed	Mitogen-activated protein kinase kinase kinase 8 (Fragment)	MAP3K8	Homo sapiens (Human)
Q5T857	Q5T857_HUMAN	unreviewed	Mitogen-activated protein kinase kinase kinase 8 (Fragment)	MAP3K8	Homo sapiens (Human)
F1R5V1	F1R5V1_DANRE	unreviewed	Mitogen-activated protein kinase kinase kinase 10 (Fragment)	MAP3K10	Danio rerio (Zebrafish) (Brachydanio rerio)
E9PID4	E9PID4_HUMAN	unreviewed	Mitogen-activated protein kinase kinase kinase 11	MAP3K11	Homo sapiens (Human)
Q16584	M3K11_HUMAN	reviewed	Mitogen-activated protein kinase kinase kinase 11 (EC 2.7.11.25) (Mixed lineage kinase 3) (Src-homology 3 domain-containing proline-rich kinase)	MAP3K11 MLK3 PTK1 SPRK	Homo sapiens (Human)
O43283	M3K13_HUMAN	reviewed	Mitogen-activated protein kinase kinase kinase 13 (EC 2.7.11.25) (Leucine zipper-bearing kinase) (Mixed lineage kinase) (MLK)	MAP3K13 LZK	Homo sapiens (Human)

Q9NYL2	M3K20_HUMAN	reviewed	Mitogen-activated protein kinase kinase kinase 20 (EC 2.7.11.25) (Human cervical cancer suppressor gene 4 protein) (HCCS-4) (Leucine zipper- and sterile alpha motif-containing kinase) (MLK-like mitogen-activated protein triple kinase) (Mitogen-activated protein kinase kinase kinase MLT) (Mixed lineage kinase-related kinase) (MLK-related kinase) (MRK) (Sterile alpha motif- and leucine zipper-containing kinase AZK)	MAP3K20 MLTK ZAK HCCS4	Homo sapiens (Human)
F1R5E9	F1R5E9_DANRE	unreviewed	Mitogen-activated protein kinase kinase kinase 21 (Fragment)	MAP3K21 Sl:CH211-120P12.3	Danio rerio (Zebrafish) (Brachydanio rerio)
E7FH13	E7FH13_DANRE	unreviewed	Mitogen-activated protein kinase kinase kinase (EC 2.7.11.25)	Sl:CH211-45C16.2	Danio rerio (Zebrafish) (Brachydanio rerio)
F1Q5J2	F1Q5J2_DANRE	unreviewed	Mitogen-activated protein kinase kinase kinase (EC 2.7.11.25)	MAP3K10	Danio rerio (Zebrafish) (Brachydanio rerio)
Q12851	M4K2_HUMAN	reviewed	Mitogen-activated protein kinase kinase kinase 2 (EC 2.7.11.1) (B lymphocyte serine/threonine-protein kinase) (Germinal center kinase) (GC kinase) (MAPK/ERK kinase kinase kinase 2) (MEK kinase kinase 2) (MEKKK 2) (Rab8-interacting protein)	MAP4K2 GCK RAB8IP	Homo sapiens (Human)
C9JCU6	C9JCU6_HUMAN	unreviewed	Mitogen-activated protein kinase kinase kinase 2 (Fragment)	MAP4K2	Homo sapiens (Human)
Q2QL34	MPV17L_HUMAN	reviewed	Mpv17-like protein (M-LP homolog) (M-LPH)	MPV17L	Homo sapiens (Human)
Q6DGV7	M17L2_DANRE	reviewed	Mpv17-like protein 2	MPV17L2 ZGC:92754	Danio rerio (Zebrafish) (Brachydanio rerio)
Q1RLZ2	Q1RLZ2_DANRE	unreviewed	Non-specific serine/threonine protein kinase (EC 2.7.11.1)	MAP4K2 MAP4K2L ZGC:136670	Danio rerio (Zebrafish) (Brachydanio rerio)
G8DKA8	G8DKA8_DANRE	unreviewed	Nrf2b	NFE2L2B NRF2B	Danio rerio (Zebrafish) (Brachydanio rerio)
Q16236	NF2L2_HUMAN	reviewed	Nuclear factor erythroid 2-related factor 2 (NF-E2-related factor 2) (NFE2-related factor 2) (Nrf-2) (HEBP1) (Nuclear factor, erythroid derived 2, like 2)	NFE2L2 NRF2	Homo sapiens (Human)
Q5TZ51	MPV17_DANRE	reviewed	Protein Mpv17	MPV17 ZGC:63573	Danio rerio (Zebrafish) (Brachydanio rerio)
P39210	MPV17_HUMAN	reviewed	Protein Mpv17	MPV17	Homo sapiens (Human)
K7ELW0	K7ELW0_HUMAN	unreviewed	Protein/nucleic acid deglycase DJ-1	PARK7	Homo sapiens (Human)
Q99497	PARK7_HUMAN	reviewed	Protein/nucleic acid deglycase DJ-1 (EC 3.1.2.-) (EC 3.5.1.-) (EC 3.5.1.124) (Maillard deglycase) (Oncogene DJ1) (Parkinson disease protein 7) (Parkinsonism-associated deglycase) (Protein DJ-1) (DJ-1)	PARK7	Homo sapiens (Human)
Q5XJ36	PARK7_DANRE	reviewed	Protein/nucleic acid deglycase DJ-1 (EC 3.1.2.-) (EC 3.5.1.-) (EC 3.5.1.124) (Maillard deglycase) (Parkinson disease protein 7 homolog) (Parkinsonism-associated deglycase) (Protein DJ-1zDJ-1) (zDJ-1)	PARK7 DJ1 ZGC:103725	Danio rerio (Zebrafish) (Brachydanio rerio)
K7EN27	K7EN27_HUMAN	unreviewed	Protein/nucleic acid deglycase DJ-1 (Fragment)	PARK7	Homo sapiens (Human)
AoA096LP96	AoA096LP96_HUMAN	unreviewed	Thioredoxin reductase 2, mitochondrial	TXNRD2	Homo sapiens (Human)
AoA096LPB7	AoA096LPB7_HUMAN	unreviewed	Thioredoxin reductase 2, mitochondrial	TXNRD2	Homo sapiens (Human)
AoA096LPD9	AoA096LPD9_HUMAN	unreviewed	Thioredoxin reductase 2, mitochondrial	TXNRD2	Homo sapiens (Human)
AoA096LPH4	AoA096LPH4_HUMAN	unreviewed	Thioredoxin reductase 2, mitochondrial	TXNRD2	Homo sapiens (Human)
AoA096LPK7	AoA096LPK7_HUMAN	unreviewed	Thioredoxin reductase 2, mitochondrial	TXNRD2	Homo sapiens (Human)
AoA182DWF2	AoA182DWF2_HUMAN	unreviewed	Thioredoxin reductase 2, mitochondrial	TXNRD2	Homo sapiens (Human)
AoA182DWF3	AoA182DWF3_HUMAN	unreviewed	Thioredoxin reductase 2, mitochondrial	TXNRD2	Homo sapiens (Human)
D3YTF8	D3YTF8_HUMAN	unreviewed	Thioredoxin reductase 2, mitochondrial	TXNRD2	Homo sapiens (Human)
E7EWK1	E7EWK1_HUMAN	unreviewed	Thioredoxin reductase 2, mitochondrial	TXNRD2	Homo sapiens (Human)

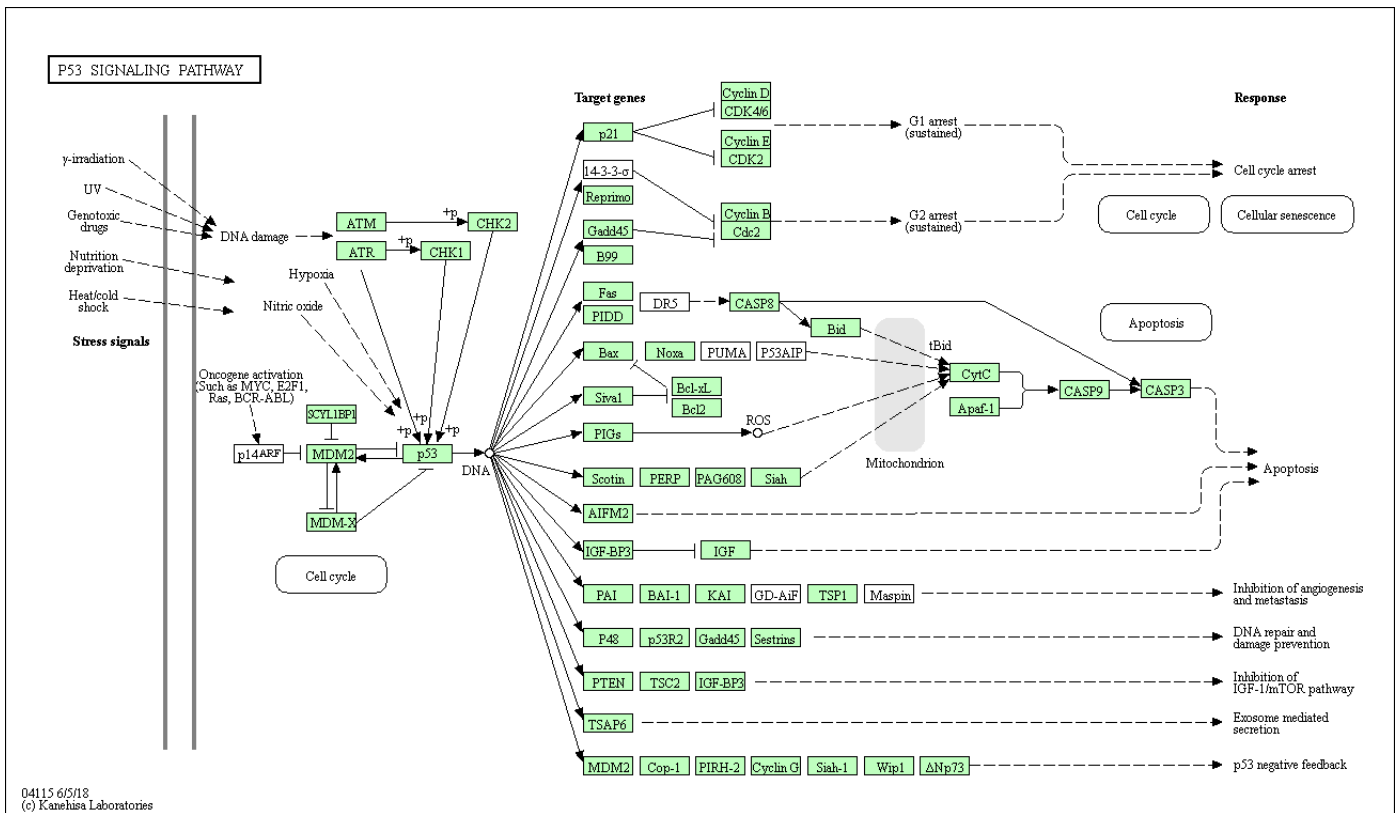
<b>Q9NNW7</b>	TRXR2_HUMAN	reviewed	Thioredoxin reductase 2, mitochondrial (EC 1.8.1.9) (Selenoprotein Z) (SelZ) (TR-beta) (Thioredoxin reductase TR <sub>3</sub> )	TXNRD2 KIAA1652 TRXR2	Homo sapiens (Human)
<b>AoAoU1RQXo</b>	AoAoU1RQXo_HUMAN	unreviewed	Thioredoxin reductase 2, mitochondrial (Fragment)	TXNRD2	Homo sapiens (Human)
<b>AoAog6LNY7</b>	AoAog6LNY7_HUMAN	unreviewed	Thioredoxin reductase 2, mitochondrial (Fragment)	TXNRD2	Homo sapiens (Human)
<b>F1QQ6o</b>	F1QQ6o_DANRE	unreviewed	Thioredoxin reductase 2, tandem duplicate 1 (Fragment)	TXNRD2.1 TXNRD2	Danio rerio (Zebrafish) (Brachydanio rerio)
<b>F1QQ6o</b>	F1QQ6o_DANRE	unreviewed	Thioredoxin reductase 2, tandem duplicate 1 (Fragment)	TXNRD2.1 TXNRD2	Danio rerio (Zebrafish) (Brachydanio rerio)

Supplementary Figure S1: KEGG pathway of oxidative phosphorylation (KEGG ID 190)

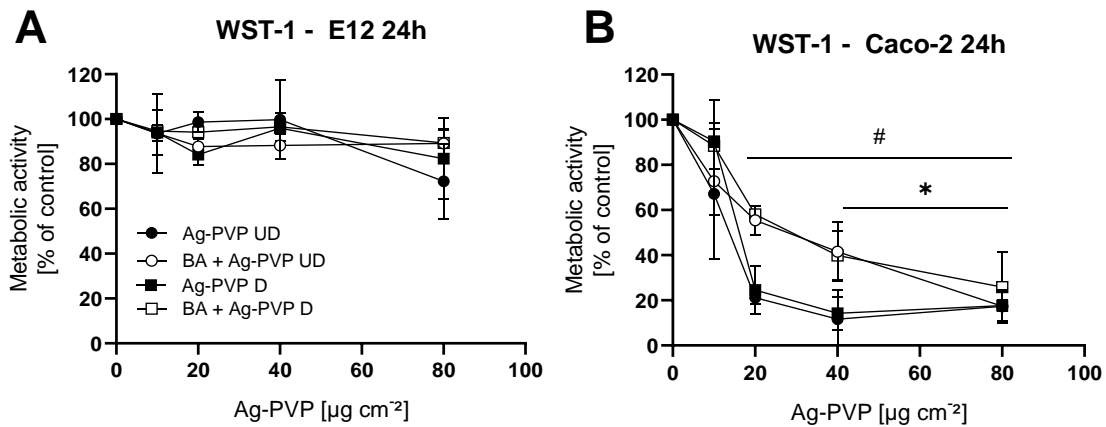




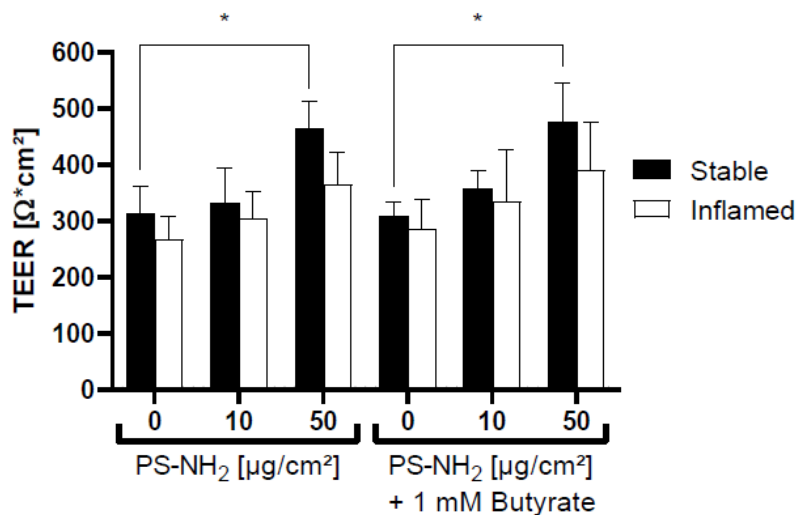
Supplementary Figure S3: KEGG pathway of P53 signalling (KEGG ID 4115)



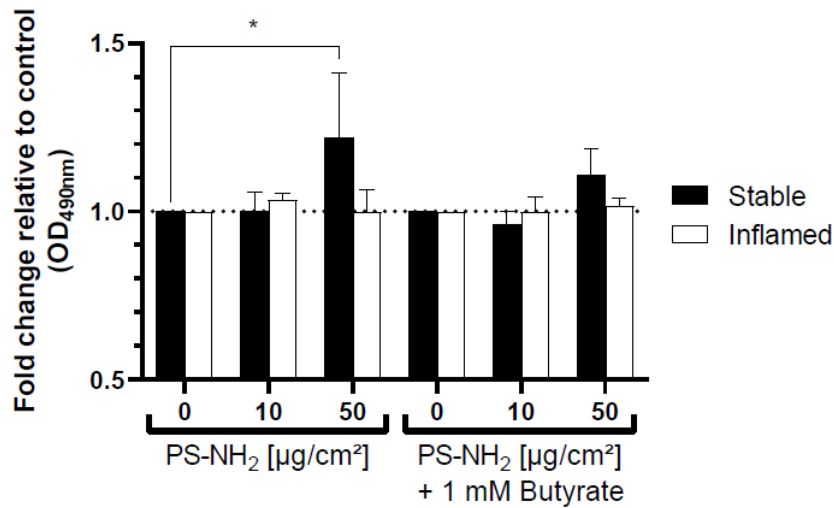
### Annex 3: Supporting *in vitro* GIT model data following ENM exposure in the presence or absence of the microbial metabolite butyric acid



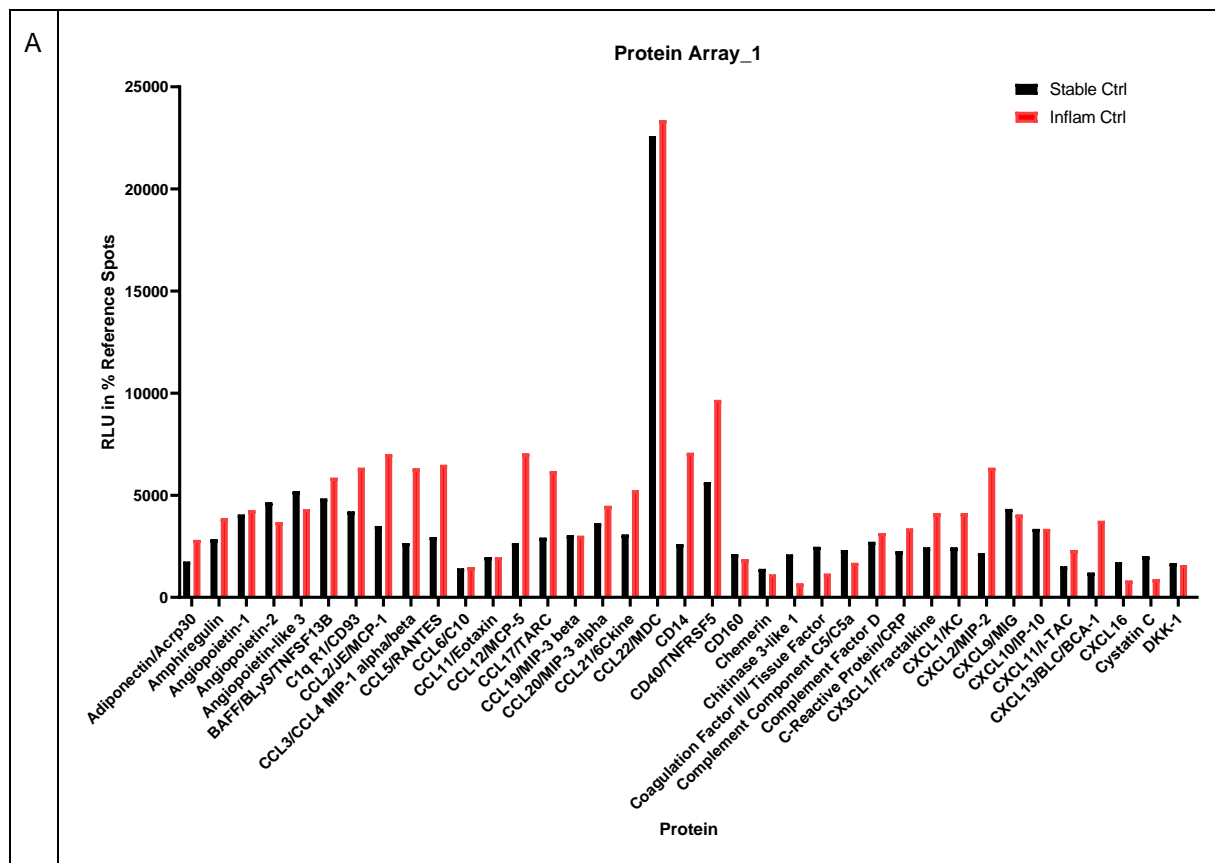
**Figure S1. Metabolic activity after 24h exposure to undigested and digested Ag-PVP ENM with and without co-incubation with 1 mM BA.** (A) E12 cells, (B) Caco-2 cells (average  $\pm$  SD of  $N \geq 3$ , # $p \leq 0.05$  cultures with BA incubation compared to respective control, \* $p \leq 0.05$  cultures without BA incubation compared to respective control. Statistical analysis with One-way ANOVA and Bonferroni *post hoc* test.)



**Figure S2. TEER (in  $\Omega \cdot \text{cm}^2$ ) after 48h stable and inflamed triple culture and 24h exposure to PS-NH<sub>2</sub> ENM with and without co-treatment with 1 mM BA** (average  $\pm$  SD of  $N=3$ , \* $p \leq 0.05$  compared to corresponding unexposed control).



**Figure S3. LDH activity in apical supernatants after 48h** stable and inflamed triple culture with 24h exposure to PS-NH<sub>2</sub> ENM in presence or absence of 1 mM BA (average ± SD, N=3, \*p≤0.05 compared to the corresponding unexposed control).



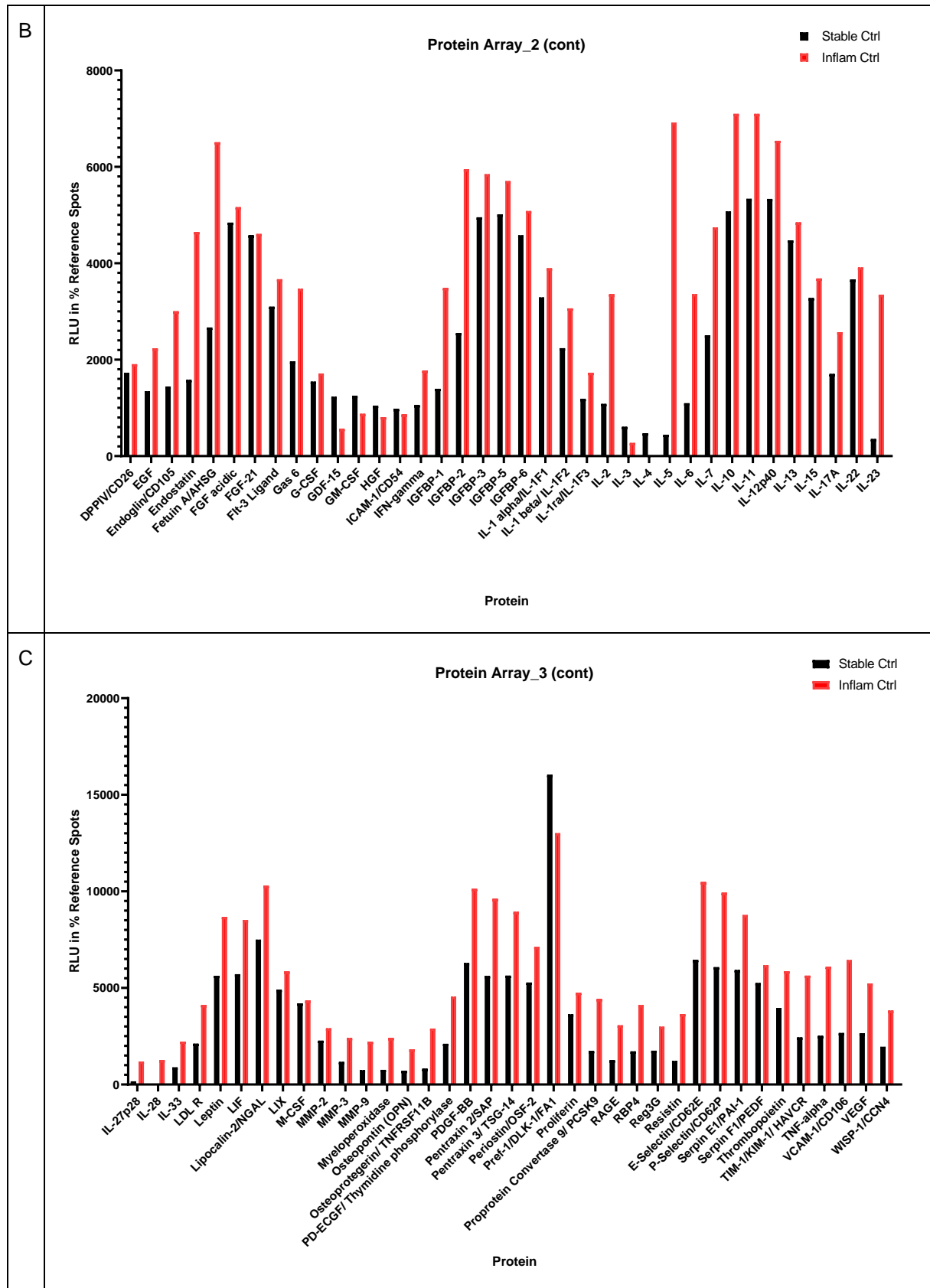


**Figure S4. Protein array profiles of stable vs inflamed triple cultures.**